Guard cell epigenomics reveals distinct abscisic acid and CO_2 triggered chromatin remodeling during stomatal movements

Charles A. Seller and Julian I. Schroeder

School of Biological Sciences
Cell and Developmental Biology Department
University of California San Diego,
La Jolla, CA 92093-0116

Guard cells integrate and respond to numerous environmental signals to control stomatal pore apertures. Chromatin structure controls transcription factor access to the genome, but whether large-scale chromatin remodeling occurs in guard cells during stomatal movements, and in response to the hormone abscisic acid (ABA), remain unknown. Here we isolate guard cell nuclei from mature Arabidopsis plants to examine whether the physiological signals, ABA and CO_2 regulate the guard cell epigenome during stomatal movements. We reveal that ABA triggers genome-wide and persistent chromatin remodeling in guard cells, roots, and mesophyll cells. DNA motif analyses uncovers binding sites for distinct transcription factors enriched in ABA-induced and ABA-repressed chromatin. We also discover bZIP transcription factors that are required for ABA-triggered chromatin opening in guard cells. We reveal that ABA and CO_2 induce distinct programs of chromatin remodeling. Our data support a model in which ABA-induced chromatin remodeling primes the genome for abiotic stresses.

INTRODUCTION

Organisms evolved mechanisms that connect the activity of their genome to the conditions in their environment. Developmental and environmental signals can impact the genome by regulating transcription factor (TF) binding to cognate DNA sequences known as cis-regulatory elements (CRE) (*1*). In eukaryotes, this regulation occurs in the context of chromatin where nucleosomes can impede transcription factor binding to target sequences (*2*, *3*). Consequently, the remodeling of chromatin structure to allow access of transcription factors to target DNA is thought to be a key step in gene regulation. Plant hormones are key signaling molecules controlling numerous aspects of plant life that coordinate genome activity with environmental conditions (*4*, *5*). Although recent studies have provided insight into how chromatin structure changes during plant development (*6*–*11*), it is unknown to what extent environmental and hormonal stimuli regulate chromatin accessibility.

Here we focus on the abscisic acid (ABA) signal transduction pathway to explore the connection between hormone signaling and chromatin structure in plants. ABA is a major plant stress hormone that accumulates in cells and tissues experiencing abiotic stress, especially those linked to the plant water-status (*12*–*14*). ABA signals through a well understood core module consisting of PYL/RCAR ABA receptor proteins, PP2C protein phosphatases, and SnRK2 protein kinases (*15*–*17*). ABA activates SnRK2 kinases, which in turn phosphorylate and thereby directly regulate downstream proteins including numerous transcription factors (*18*–*24*). Consequently, ABA triggers the differential expression of thousands of genes in the *Arabidopsis thaliana* genome (*4*, *25*–*27*). However, it remains unclear, especially at the genome scale, whether ABA signaling reshapes chromatin structure, and how ABA-regulated TFs might function in the context of chromatin.

One well known action of ABA is to trigger the closure of the stomatal aperture. Stomata are small pores on the surface of the leaf that mediate gas exchange and are formed by a pair of specialized epidermal cells known as guard cells. Guard cells perceive and respond to multiple environmental and hormonal cues in order to optimally regulate the size of the stomatal pore (*28*–*30*). For instance, some signals such as elevated atmospheric CO_2, ABA, and the immune elicitor Flg22 trigger stomatal closure while reduced CO_2, light and heat trigger stomatal opening. Because of their exquisite environmental reactivity, guard cells are an excellent model cell system to investigate how different signals regulate chromatin structure in a cell-type specific manner in response to physiological stimuli. Although the recent application of single-cell RNA-seq to *Arabidopsis* has expanded our understanding of gene regulation, these studies often focus on plate-grown seedlings (*31*, *32*) and/or resulted in datasets with limited representation of guard cells (*33*, *34*). To apply epigenomic techniques to the question of how guard cells respond to different stimuli new protocols are needed that can isolate large numbers of pure guard cells from soil grown plants, a more relevant setting for physiological studies.

In this paper, we describe the development of an approach to purify guard cell nuclei and by deploying this method, uncover how guard cell chromatin structure changes in response to different stimuli that drive stomatal movements. We profiled the chromatin and transcriptional reprogramming in response to ABA and in three different developmental contexts – roots, mesophyll cells, and guard cells. We map thousands of loci that gain or lose chromatin accessibility in response to ABA and link these regions to co-regulated transcripts uncovering a critical role for chromatin dynamics in controlling ABA-dependent transcription. Furthermore, we show that genome-wide and persistent changes to chromatin structure accompany ABA-induced stomatal closure and that four related bZIP transcription factors known as ABRE Binding Factors (ABFs) are required for initiating the majority of ABA-induced chromatin

opening. In contrast, we implicate a family of related bHLH-type TFs known as ABA-Kinase Substrates (AKSs) in the maintenance of open chromatin upstream of ABA-repressed genes. Finally, we show that in guard cells, changes to atmospheric CO_2-concentration trigger distinct chromatin remodeling and gene regulatory programs from those mediated by abscisic acid.

RESULTS

ABA induces rapid and genome-wide chromatin remodeling in roots

As an initial test of the relationship between ABA and chromatin we focused on *Arabidopsis thaliana* seedlings. To measure changes to chromatin structure we combined the fluorescence activated nuclei sorting (FANS) with the Assay for Transposase-Accessible Chromatin with sequencing (ATAC-seq), a quantitative measurement of chromatin accessibility across the genome (*35*, *36*). Seedlings were treated with 50 uM ABA for 4hrs after which 50,000 nuclei per sample were isolated using FANS (Fig. S1A). We called 25,892 ATAC-seq peaks across all whole seedling libraries, genomic regions coinciding with these peaks are known as Accessible Chromatin Regions (ACRs) and predominantly aligned with upstream regulatory regions in the genome (Fig. S1B-D). In contrast, ATAC-seq reads derived from purified genomic DNA did not cluster into defined peaks (Fig. S1B). We first treated whole seedlings with ABA and profiled chromatin accessibility after 4 hours. Differential analysis revealed hundreds of regions that significantly gain and lose accessibility in response to ABA (Fig. 1A).

To capture the dynamics of ABA-induced chromatin remodeling we focused on roots which can rapidly take up ABA from their surroundings (*37*, *38*). Using FANS, we isolated root nuclei at three different timepoints following ABA treatment (after 45, 120, and 240 minutes) and performed ATAC-seq. Differential analysis revealed that ABA triggers time-dependent changes in chromatin accessibility in roots. Heatmaps centered over these ABA regulated ACRs illustrate the progressive impact of ABA on chromatin structure, with more regions of the genome changing in ATAC-signal over time (Fig. 1A,B). We observed significant changes to chromatin after only 45 minutes of ABA treatment, with 119 ACRs located in upstream regulatory regions gaining accessibility and 49 losing accessibility (Fig. 1C,E). After 4 hours, ABA had activated 972 ACRs and repressed 734 ACRs. Interestingly, we found that ABA-regulated ACRs tend to be located more distally (> 2kb) than static regions (Fig. 1D). ABA-induced ACRs were associated with downstream genes enriched for gene ontology (GO) terms such as “response to water deprivation”, “response to osmotic stress”, and “response to abscisic acid”.

To explore the role of specific transcription factors in orchestrating these changes we performed DNA motif analysis using a set of motifs empirically generated by the in vitro DNA binding assay DAP-seq (*39*). We found that motifs recognized by ABF/AREB transcription factors such as ABF1/2/3/4 and ABI5 were highly enriched in ABA-induced ACRs (Fig. 1F, example ABF1, p = 1e-49). In contrast, we found that ABA-repressed ACRs showed enrichment for motifs recognized by the related bHLH type transcription factors AKS1, AKS3, and bHLH80 (Fig. 1F, example AKS1, p = 1e-50). Notably, both ABF and AKS proteins are direct targets of ABA-regulated SnRK2 kinases (*18*, *20*). Previous research has shown a role for ABA-dependent inhibition of bHLH-type AKS transcription factors in the down-regulation of the of a guard cell K^+ channel *KAT1* transcript (*20*, *40*). Interestingly, our findings suggest a larger role of the AKS clade of closely related bHLH proteins in the regulation of ABA-repressed genes. We conclude that ABA can trigger rapid and genome-wide chromatin remodeling in root tissue.

Revealing guard cell specific patterns of chromatin accessibility

Encouraged by our findings in whole seedlings and roots we next decided to investigate the effect of ABA on chromatin in mature guard cells. We first developed a FACS-based strategy to purify guard cell nuclei from soil-grown plants. Nuclei were labeled by expressing the histone H2B fused to GFP under the control of the guard cell specific *pGC1* promoter (*41*, *42*). We first confirmed the guard cell specificity of the H2B-GFP fusion in transgenic lines using fluorescence microscopy (Fig. 2A). We found that chopping leaf material in lysis buffer using a razor blade was insufficient to release GC nuclei, possibly due to their strong cell walls. Instead, we prepared lysates by first enriching for epidermal tissue by blending the leaves of ~40 5 to 6-week-old plants and then ground snap-frozen tissue using a mortar and pestle. DAPI stained crude nuclei preparations were then analyzed using FACS (Fig S2A). Using this approach, we could define a clearly separated GFP-positive population among all detected nuclei (Fig. 2B, Fig. S2B). In contrast to many other cell types in the Arabidopsis leaf, guard cells are diploid and GFP-positive nuclei from pGC1:H2B-GFP expressing plants had a 2n DNA content while GFP-negative nuclei were distributed among higher ploidy levels (Fig. 2C). This method allowed us to obtain ~30,000 guard cell nuclei with an estimated purity of 98% (Fig. S2C) from the leaves of 40-50 plants. To assay guard cell chromatin structure, nuclei isolated using this method were used to generate ATAC-seq libraries. The resulting libraries were of high quality with clear concentration of peaks in annotated upstream regulatory regions (Fig. S2D), enrichment of open chromatin fragments (< 100 bp) immediately upstream of transcription start sites (Fig. S2E), strong correlation between biological replicates (Fig. S2F), and high FRiP (fraction of reads in peaks) scores (Table S1).

In parallel, we generated ATAC-seq samples from root nuclei and from FANS-isolated mesophyll nuclei labeled by expression of H2B-GFP from the promoter of the mesophyll expressed Rubisco small subunit 2B gene (Fig S3A-C) (*6*). For each tissue/cell-type we compared ATAC-seq libraries derived from three biological replicates. We identified 33,212 ATAC-seq peaks across all samples and called cell-type specific peaks using pairwise differentially accessibility analysis. Although most ATAC-seq peaks were common to all cell types, we found 3272 guard cell specific ACRs, 1472 mesophyll specific ACRs, and 3364 root specific ACRs. Heatmaps centered over these regions highlight characteristics of cell/tissue specificity in the observed patterns of chromatin accessibility (Fig. 2D). Importantly, biological replicates clustered together in principal component analysis with samples derived from the same cell type underscoring the robustness of this approach (Fig. 2E).

To evaluate the relationship between guard cell specific chromatin accessibility and gene expression we performed RNA-seq on both whole leaves and guard cell-enriched samples. We found that regions with high chromatin accessibility specifically in guard cells were associated with elevated transcript levels from the adjacent downstream genes indicating that we are identifying functional cis-regulatory elements (CREs) (Fig. 2F). By connecting guard cell specific ACRs with downstream guard cell enriched transcripts we were able to define a set of 867 putative regulatory elements preferentially active in guard cells (Table S2). Examination of individual gene loci like the guard cell specific genes *KAT1* (*43–45*) and *SLAC1* (*46*, *47*) illustrated the connection between increased upstream accessibility and increased transcript (Fig. 2G). By contrast, the mesophyll specific gene *AOC1* showed had high chromatin accessibility in mesophyll cells, but minimal upstream ATAC-seq signal in guard cells. TF binding motif analysis of guard cell specific ACRs returned motifs with strong similarity to known guard cell transcriptional regulators such as FAMA (*48*), EDT1, and DOF (*49*) and BPC (*11*) type TFs (Fig. 2H). In summary, we have developed a robust protocol for isolating pure populations of guard cell nuclei allowing us to discover CREs that define guard cells.

ABA induces persistent chromatin remodeling in guard cells during stomatal closure

We next asked whether epigenomic reprogramming occurs during ABA-induced stomatal closure. Soil grown 6-week-old plants were sprayed with 50 uM ABA and after 3 hours, we confirmed a stomatal response by infrared photography (Fig. 3A). To determine if our ABA treatment led to significant transcriptional changes we performed RNA-sequencing on both whole leaf samples (Fig. S4A) and guard cell enriched samples (Fig. 3B). We observed that ABA triggered the differential expression of thousands of transcripts in both whole leaves and guard cells (2316 upregulated and 1529 downregulated - Fig S4A,B). As expected, ABA-induced genes are enriched for the pathways “response to water deprivation” (p_value = 1.7e-22), “response to abscisic acid” (pvalue = 4.47e-18), and “response to salt stress (Fig. S4D). Although most of the transcriptional changes induced by ABA were shared between guard cells and whole leaves, we found that 22.7% (488) of ABA-induced transcripts and 42.7% (673) of ABA-repressed transcripts were specific to guard cells (Fig. S4C, Table S3). For instance, ABA induced expression of the gene *HAI2* in both whole leaves and guard cells while the ABA-regulated expression of the major facilitator protein-encoding *AT2G37900* and the wax biosynthesis enzyme-encoding *AAE9* (*50*) were only evident in guard cells (Fig. S4E).

To evaluate if ABA changed chromatin accessibility and whether these changes are sustained over time following a single treatment, we isolated guard cell nuclei at 4 hours and 24 hours after spraying (Fig. 3A). We generated ATAC-seq libraries from three biological replicates per time point, and PCA results showed that samples clustered together according to treatment (Fig. S5A). Differential chromatin accessibility analysis found that ABA extensively reshapes chromatin structure in guard cells with 2260 ACRs gaining accessibility and 1662 ACRs losing accessibility across the treatment time course (Fig. 3C, Table S4). We next analyzed the temporal characteristics of this response by comparing the ATAC-seq datasets from the 4-hour and 24-hour timepoints. Our results allowed us to define three categories of ABA-regulated ACRs – early, sustained, and late (Fig. 3D). Strikingly, we found that 1091 of the 2028 (53.8%) ACRs opened by ABA at 4 hours remained open after 24 hours. Of the 990 ACRs closed by ABA at 4 hours 614 (62%) remained closed at 24 hours. Additionally, we found 232 ACRs gained and 670 ACRs lost accessibility only 24 hours after ABA treatment (Fig. 3D).

We next performed TF binding motif analysis on these three categories of peaks using a set of DAP-seq derived motifs (*39*) restricted to those TFs with guard cell expression in our RNA-seq datasets. Both early and sustained ABA-induced ACRs had strong enrichment for motifs recognized by ABRE- binding TFs including ABI5, ABF1,2, and 3 (Fig. 3F). Interestingly, we found that the motifs recognized by CBF2, CBF3, and MYB61 (*51–53*) were only enriched in early ABA-induced ACRs. ABA-repressed ACRs showed strong enrichment for motifs recognized by the related bHLH-type TFs AKS1, AKS3, and FBH1 in both sustained and late categories. In contrast, MYB96 motifs were enriched only in late appearing ABA-repressed ACRs (Fig. 3G). Collectively, our results demonstrate that ABA can induce persistent changes to chromatin in guard cells and expose the temporal regulation of different TFs during this response.

Consistent with our observations in seedling roots, we found that ABA-regulated ATAC-seq peaks in guard cells reside further away from transcription start sites (TSS) than non-regulated peaks (> 2kb), indicating that distal regulation may be a characteristic of ABA-controlled CREs (Fig. S5C). ABA-induced ACRs in guard cells are clearly associated with downstream genes that are upregulated transcriptionally by ABA, while ABA-repressed ACRs are associated with genes downregulated by ABA (Fig. 3E). Examination of individual genes like the ABA-upregulated *DTX37 (AT1G61890)* and the ABA-downregulated *MYB60* (*54*) illustrate the connection between upstream chromatin accessibility and transcript levels (Fig. 3H).

Interestingly, we found that ABA modifies chromatin accessibility upstream of many known regulators of stomatal conductance including *KAT1*, *NCED3*, and *HT1* (*55*) as well as many other genes with no known stomatal functions (Fig. S6, Table S4). Furthermore, by comparing ABA-induced ACRs from guard cells, mesophyll cells (Fig. S3E-G), and root cells (Fig. 1C-G) we uncovered significant tissue/cell-type specificity in this response (Fig. 3I). Interesting, we found that ABA had a much larger impact on chromatin accessibility in guard cells than in the other cell types (2028 ACRs compared with 972 in roots and 782 in mesophyll).

By comparing our guard cell ATAC-seq data with recent genome-wide DAP-seq profiles generated for ABF1/2/3/4 (*56*) we found that many ABF binding sites reside within ABA-induced ACRs. In contrast, ABA-repressed ACRs in guard cells significantly overlapped with the in vitro binding sites of AKS1, AKS3, and the related bHLH transcription factor bHLH80/FBH1. Additionally, unbiased de novo motif discovery (*57*) returned motifs similar to ABF1 and AKS3 binding sites as the most enriched in ABA-activated and ABA-repressed ACRs, respectively (p = 1e-119 and p = 1e-57). Metaplots of ATAC-seq signal centered over peaks containing these motifs further supported our observation that ABA elevates chromatin accessibility at ABF binding sites and represses chromatin accessibility at AKS binding sites (Fig. S5B). Interestingly, ABA repressed chromatin accessibility upstream of AKS3 and decreased the associated transcript levels in guard cells (Fig. 3J). To determine if AKS3 protein levels are impacted by ABA we expressed GFP tagged AKS3 under its native regulatory sequence. We observed that ABA treatment decreased GFP-AKS3 signal in guard cells (Fig. 3K). In conclusion, we show that ABA drives large scale changes to chromatin structure in guard cells and implicate major roles for the activation of ABFs and inhibition of AKSs in this response.

ABF transcription factors are required for ABA-induced chromatin opening in guard cells

The mechanisms that cause ABA-specific chromatin opening are unknown. Given the strong enrichment of ABF binding motifs in ABA-activated ACRs, and their coincidence with ABF *in vitro* binding sites, we wondered if these TFs might be required for reshaping chromatin during ABA-induced stomatal closure. To test this, we used the *abf1/2/3/4* (*abfx4*) quadruple mutant which lacks four related ABF proteins that are prominent during vegetative growth (*21*, *22*). We first performed RNA-seq following ABA treatment on leaves from 6-week-old *abf1/2/3/4* (*abfx4*) mutant plants (Fig. S7A). Strikingly, of the 2469 transcripts that are upregulated by ABA in wild type leaves, 2030 (~82%) depend on ABF1-4 (Fig. S7B). Interestingly, although ABA increased *ABF1/2/3/4* transcript levels in guard cells we did not find that ABA altered chromatin accessibility in the upstream regions near the *ABF1/2/3/4* genes (Fig. S7C). We conclude that ABF1-4 are required for the bulk of ABA-induced gene expression in mature leaf tissue. Plants lacking *ABF1/2/3/4* (*abfx4*) are highly sensitive to drought stress and lose water faster than wild type plants in detached leaf assays (*22*). Consistent with these prior findings, we observed that *abfx4* mutant plants exhibited higher steady-state stomatal conductance than *Col-0* control plants (Fig. S7D).

In non-stressed conditions, guard cells have a higher ABA concentration than other leaf cell types (*38*, *58*). Recent studies have provided evidence for basal ABA signaling in guard cells and defined important roles for basal ABA in stomatal function (*59*, *60*). By generating guard cell FANS lines in an abfx4 mutant background (Fig. S8A) we were able to assess the impact of the loss of ABF1/2/3/4 on guard cell chromatin in non-stressed plants. In the absence of ABA treatment, we observed minimal differences in genome-wide patterns of chromatin accessibility between WT and abfx4 guard cells (Fig S8B, C) suggesting that basal ABA signaling in guard cells may regulate mainly post-transcriptional stomatal closing mechanisms, but does not significantly regulate chromatin structure. Next, we asked if the ABF1-4 are required for the

ability of ABA to reshape chromatin structure. Strikingly, loss of *abf1/2/3/4* strongly impaired ABA-induced chromatin opening in guard cells but had less impact on ABA-triggered chromatin closing (Fig. 4A). Of the 2080 ABA-induced ACRs, 1508 (~72%) required ABF1/2/3/4 for gained accessibility (Fig. 4B). As expected, ABF-dependent ACRs were strongly enriched for ABREs (p = 1e-104). Examination of individual loci revealed a close connection between abf-dependent increases in upstream chromatin accessibility and abf-dependent transcription (Fig. 4C).

We next performed TF motif analysis on ABF-dependent and ABF-independent regions of ABA regulated open chromatin. As expected, ABF-independent ACRs were depleted for ABRE motif enrichment but retained enrichment for AKS1, AKS3, and bHLH80 motifs (Fig. 4G). Additionally, we found that CBF1, CBF2, and CBF3 motifs retained enrichment in ABA-induced ACRs in *abfx4* mutant guard cells. TF binding motifs are often information poor and the presence of a motif at a genomic location does not always lead to TF action. In vitro binding experiments for ABF1-4 on naked genomic DNA uncovered 14454 binding sites, but only 1315 resided within ABA-induced ACRs in guard cells (Fig. 4D). However, ABA-induced chromatin opening at ACRs containing ABF-binding sites was strongly impaired in *abfx4* mutant guard cells (Fig. 4E). We reasoned that chromatin structure may determine which motifs are functional. To test this idea, we examined if the presence of ABF DAP-seq binding sites could predict ABA-activated transcription. Using guard cell RNA-seq data, we found that ABF binding sites that reside in regions of ABA regulated open chromatin are more strongly associated with downstream ABA-induced genes than the ABF binding sites outside of these regions (Fig. 4F).

To examine the temporal characteristics of ABF-dependent chromatin remodeling we focused on roots where ABA can reshape chromatin by 45 mins (Fig. 1C). We performed ATAC-seq on isolated *abfx4* mutant root nuclei over an ABA treatment time course and found that ABA fails to drive progressive chromatin opening in this background (Fig. S8). In *abfx4* mutant roots, 45 mins of ABA treatment induced only 6 ACRs compared to 189 in wild type roots. By 2 hours of ABA treatment, only 47 ABA-induced ACRs were present in abfx4 mutants compared with 642 in wild type (Fig. 4H and Fig. S8A). Consistent with our observations in guard cells (Fig. 4A), ABA repressed a similar number of ACRs in the absence of ABF1/2/3/4 (Fig. 4H and Fig. S8A). Collectively, these results demonstrate that the ABF1/2/3/4 transcription factors are required for triggering genome-wide chromatin opening in response to ABA.

ABA and changes to atmospheric CO_2 concentration induce distinct chromatin remodeling programs in guard cells

Because we observed that ABA has extensive effects on chromatin accessibility in guard cells, we wondered whether chromatin structure may respond to other stimuli that drive stomatal movements. Here we focus on changes to atmospheric CO_2 concentration. Exposure of plants to low CO_2 stimulates stomatal opening while high CO_2 drives stomatal closure (Fig 5A). The exact role of ABA signaling during CO_2 induced stomatal responses is unclear and is a matter of some debate (*59*–*61*). Recent studies suggest that although high-CO_2 induced stomatal closure requires basal ABA signaling it does not involve further SnRK2 kinase activation (*59*, *61*). Comparing how these signals impact genome activity could provide new insight into whether and how the mechanisms underlying guard cell responses ABA and CO_2 to them may differ.

To generate low and high CO_2 guard cell ATAC-seq libraries we exposed 6-week-old plants to either 100 ppm CO_2 or 1000 ppm CO_2 for 4 hrs, two treatments that induce robust stomatal responses (Fig 5B). Surprisingly, in contrast to the extensive effect of ABA on chromatin accessibility in guard cells (Fig. 5C), we observed smaller changes in response to low CO_2 (Fig.

5D). and minimal changes following treatment with high CO_2 (Fig. 5E). Following exposure of plants to 100 ppm CO_2, 372 ACRs gained accessibility and 591 ACRs lost accessibility while treatment with 1000 ppm CO_2 induced only 10 ACRs and repressed 104 (Table S3). Heatmaps of ATAC-seq signal at ABA and Low CO_2-regulated regions highlighted the specificity of these responses (Fig. 5F). PCA results comparing our guard cell ATAC-seq datasets from different conditions further support these findings and revealed little difference in chromatin accessibility between control and high CO2 treatments (Fig. 5G). Examination of individual loci highlights the specificity of these responses, for instance chromatin opening upstream of *ERF113* only occurred in response to ABA while the upstream regions of the genes *ALMT6* and the PP2C-encoding *AT2G25070* gain accessibility only in response to low CO2 (Fig. S10B-E).

Analysis of the set relationships among ABA, low CO_2, and high CO2 regulated ACRs revealed little overlap suggesting that these stimuli control distinct cis-regulatory elements in the genome (Fig. S10A). We did find significant overlap between ABA-induced and low CO_2-repressed ACRs and between ABA-repressed and low CO_2-induced ACRs. Interestingly, ABA repressed chromatin accessibility upstream of *HT1*, *BLUS1*, and *CBC2* (*62*), all key positive regulators of low CO_2 induced stomatal opening (Fig. 5H). These data indicate that chromatin remodeling represents an important cross talk point for these stimuli, ensuring robust stomatal closing or opening, depending on the physiological conditions. For instance, ABA-repressed chromatin accessibility upstream of *ALMT6* and *CBP60F*, while low-CO_2 treatment enhanced accessibility (Fig. S10D,E). Additionally, many genes downstream of low-CO_2 activated ACRs encode transcripts that are downregulated by ABA. genes DNA binding motif analysis further emphasized the distinct regulatory impacts of changes in CO_2 concentration and ABA on the genome. In contrast with ABA-induced ACRs, we did not find enrichment of ABF binding motifs in low or high CO_2 regulated chromatin (Fig 5I). Instead, low CO_2 gained ACRs were enriched for motifs recognized by C2C2dof-type TFs that are oppositely enriched only in ABA-repressed ACRs. Collectively, our data demonstrate how different signals that control stomatal movement deploy distinct gene regulatory programs in guard cells.

DISCUSSION

Abscisic acid triggers changes in gene expression but whether this transcriptional response depends on chromatin remodeling remained unknown (*5*). Here, we reveal massive ABA-induced chromatin remodeling pointing to an orchestrated reprogramming of the Arabidopsis epigenome by specific sets of transcription factors. Furthermore, we show distinct patterns in ABA-triggered chromatin remodeling in seedling roots, mesophyll cells and guard cells.

Guard cell regulation of stomatal aperture size is essential for plant survival under drought stress. Such regulation requires that the guard cells forming the stomatal pore integrate numerous physiological and environmental cues. In this study, we profiled genome-wide chromatin accessibility in tens of thousands of guard cells isolated from soil-grown plants exposed to different stimuli that trigger stomatal movements. Our results lead us to propose that guard cell ABA signaling controls the balance between two opposing chromatin states that are enforced by two major groups of transcription factors (Fig. 6). Under unstressed conditions, AKS proteins maintain open chromatin at upstream regulatory regions of ABA-repressed genes while ABA-activated genes are kept silent by closed chromatin. Under abiotic stress such as drought, ABA levels rise in guard cells thereby activating SnRK2 kinases which subsequently inhibit AKSs and activate ABFs. This would then drive the system towards a new state characterized by open chromatin upstream of abiotic stress-activated genes and close chromatin upstream of stress-repressed genes.

We found that ABA induces extensive and cell-type specific chromatin remodeling and that guard cells possess a much more extensive response than mesophyll and root cells (Fig. 3I). The plant hormone cytokinin also modulates chromatin structure (*63*) but its impact on the accessible genome was smaller than what we observed for ABA (760 cytokinin-regulated ACRs and 2721 ABA-regulated ACRs). By performing TF-binding motif enrichment and analyzing published DAP-seq data, we implicated the bZIP transcription factors ABF1/2/3/4 in ABA-induced chromatin remodeling in guard cells (Fig. 3F and Fig. S5B). Our experiments in *abf1/2/3/4* quadruple mutant guard cells demonstrate that these four transcription factors are essential for the majority of ABA-triggered chromatin opening (Fig. 4) and that in their absence, guard cells fail to establish and or maintain an ABA-induced pattern of chromatin accessibility. Furthermore, experiments in root nuclei show that in *abf1/2/3/4* quadruple mutants, even early ABA-induced chromatin remodeling events are strongly impaired (Fig. 4H and Fig. S8), suggesting that ABFs initiate chromatin opening. How ABFs accomplish chromatin opening remains to be determined, but existing literature could be interpreted to support two possible and not necessarily mutually exclusive explanations. (1) Although nucleosomes can restrict TF binding to DNA, some TFs, known as pioneer factors (*64*, *65*), possess the ability to bind their target sequences even within inaccessible chromatin regions. At present, only a handful of pioneer factors have been documented in plants (*66*), but research in mammals has shown that bZIP proteins such as CEBPA can act as pioneer factors (*67*). While our data is consistent with ABFs acting as pioneer factors, future biochemical experiments reconstituting ABF binding to nucleosomal DNA are needed to investigate this model. (2) Additionally, ABFs may recruit chromatin modifying proteins to target sequences which could increase chromatin accessibility. Interestingly, several such molecules including the SWI/SNF ATPase BRM (*68*, *69*) and the histone deacetylase HDA9 (*70*) interact with known ABA signaling components. Currently, no direct evidence exists linking ABFs to chromatin remodeling or histone modifying enzymes exists.

Beyond ABF1/2/3/4, our analyses implicated additional TFs in ABA-dependent genome reprogramming (Fig. 3F and 3G), which correlates with prior research showing that ABA regulates the binding of multiple transcription factors. Notably, our data suggest that the related bHLH transcription factors known as AKSs play a larger role in the regulation of ABA-repressed genes than was previously thought. Prior research had shown that SnRK2 kinase-dependent inhibition of AKS1/2 was required for the ABA-dependent transcriptional repression of the K+ ion channel gene *KAT1* in guard cells (*20*). Interestingly, we found that 302 ABA-repressed ACRs contain DAP-Seq binding sites for AKS1/2/3 overlap with (Fig. S5B). This observation was further supported by de novo motif analysis (Fig S5C). AKS1 and AKS2 are inhibited by direct ABA-dependent SnRK2 phosphorylation, but their expression was not controlled by ABA signaling (*40*). We found that in guard cells, ABA represses both AKS3 transcript and protein levels implying that ABA-dependent inhibition of AKS proteins occurs through multiple mechanisms (Fig. 3J and K). Moreover, we observed that ~30% of ABA-gained ACRs (622 ACRs) still open in abfx4 mutant guard cells in response to ABA (Fig. 4B). These ABF-independent regions were enriched for CBF1/3 binding motifs, implicating CBF transcription factors in a larger role in ABA signal transduction in guard cells (Fig. 4G). Finally, although ABA-induced chromatin opening is severely impaired in *abf1/2/3/4* quadruple mutant guard cells, we cannot exclude the possibility that other ABRE-binding TFs in particular ABI5 (*71*, *72*) participate in this process as well.

Elevation in the CO_2 concentration in leaves triggers rapid stomatal closing (*30*). The extent to which elevated atmospheric CO_2 signals through the ABA signal transduction pathway is currently under debate. Different research groups using the same mutants have come to different conclusions regarding direct CO_2 signaling via early ABA receptor/SnRK2 kinase

pathway during CO_2-induced stomatal closure. Our results exposed major differences in how guard cells interpret these stimuli. Interestingly, in contrast to the extensive and persistent changes to chromatin structure induced by ABA (Fig. 3), exposure to elevated CO_2 has minimal impact on genome-wide chromatin accessibility in guard cells (Fig. 5). While ABA regulates chromatin accessibility at 3018 ACRs in the genome, we found that only 114 ACRs were regulated by elevated CO_2 (Fig 5C-E). Additionally, the strong enrichments of ABF binding motifs in gained ACRs and AKS binding motifs in lost ACRs evident following ABA treatment are absent during the response to elevated CO_2 (Fig. 5I). The disparity between these two signals at the level of chromatin mirrors the disparity between characteristics of their respective physiological responses. Unlike ABA- and drought-triggered stomatal closure, elevated CO_2-induced stomatal closure is rapidly reversed upon return to ambient CO2 (*59*). Our findings also support crosstalk between ABA and low CO_2 signaling, notably we uncovered that ABA triggered chromatin closing upstream of key positive regulators of low CO_2 induced stomatal opening (Fig. 5H).

Finally, our results may open new avenues for investigation into two poorly understood features of stomatal biology. Studies in multiple plant species have documented a phenomenon referred to as stomatal "memory" (*73*, *74*). Following drought stress and re-watering, typically plants exhibit delayed and/or slow re-opening of stomata despite rapid recovery of plant water status. Furthermore, guard cells display transcriptional memory where repetitive dehydration stress leads to altered transcript levels in subsequent stress events (*75*–*77*). This altered response can exist for several days in Arabidopsis and genetic analysis showed that this response can be impaired in mutants lacking key ABA-signaling components (*76*). We found that ABA triggered changes to chromatin accessibility in guard cells that can persist for up to 24 hours, which could prime the genome for subsequent abiotic stress exposure (Fig. 3). These shifts occurred at thousands of locations in the genome including upstream of many genes known to regulate stomatal movements as well as many genes with potential functions in stomatal physiology that could be the basis for future studies (Fig. S6 and Table S3). ABA-triggered changes to guard cell chromatin structure provide a basis for long-term reprogramming of the guard cell genome for abiotic stress survival. We envision that these sustained changes to chromatin structure may store the experience of drought stress and contribute to long-term adjustments of stomatal function.

METHODS

Plant material and growth conditions

The Columbia-0 (Col-0) accession of *Arabidopsis thaliana* was used as the wild-type background. Experiments on seedlings were conducted using plants germinated and grown on 1/2 Murashige and Skoog (MS) media (pH 5.8) supplemented with 1% Phyto-agar plates. Experiments using mature plants were conducted using plants grown in soil (Sunshine Mix #1) filled plastic pots placed in a growth chamber (Conviron) under a 12hr-12hr light-dark cycle, a light intensity of 100 µmol m^{-2} s^{-1}, a temperature of 22 C, ambient [CO_2], and a relative humidity of 65%. To minimize the impact of environmental variation all experiments were performed on plants grown in two identical growth chambers equipped with [CO_2] control.

ABA treatments in plate-based experiments were performed using a mesh (100 µm polyester) transfer method to transfer seedlings in mass to treatment plates. ABA treatments on soil grown plants were performed by spraying plants with 50 µM ABA (Sigma cis/trans-abscisic acid) diluted with 0.01% Silwet (in water). To assess treatment responses, leaf temperature was measured using an infrared thermal imaging camera (T650sc; FLIR).

Plasmid DNA and plant transformation
Constructs for cell-type specific nuclear sorting were prepared using multi-site gateway technology (Invitrogen). The ORF encoding histone H2B (AT5G22880) was cloned in a pDONR221 entry vector. Cell type specific promotors were cloned from the Arabidopsis genome into gateway entry vectors. Final plant transformation constructs were generated by performing multisite gateway recombination into the pP7m34GW destination vector. The plasmid for expressing GFP-AKS3 under the AKS3 endogenous promotor was generated using GreenGate cloning (*78*). The cloned AKS3 upstream regulatory sequence was defined using guard cell ATAC-seq data. Primer sequences are available in Table S4. Constructs were transformed into A. thaliana Col-0 plants using the floral dipping technique with *Agrobacterium tumefaciens* strain GV3101.

Microscopy
Plant leaves were mounted on conventional glass microscope slides in water with the abaxial epidermal layer against the coverslip. GFP fluorescence was recorded using a Eclipse TE2000-U (Nikon, Tokyo, Japan) spinning disc confocal microscope. Constant gain and exposure times were used for each experiment when comparing treatments/samples. Images were processed for publication using Fiji software.

Time resolved stomatal conductance measurements
For gas exchange experiments, *Col-0* and *abfx4* mutant plants were grown together in the same growth chamber to minimize biological variation. Intact leaves of six-week-old plants were used for gas exchange experiments and stomatal conductance was measured using a Licor 6400 infrared gas exchange analyzer equipped with a leaf chamber (LI-COR Biosciences). Before beginning measurements, clamped leaves were equilibrated for 45-60 mins at 150 µmol m^{-2} s^{-1} light intensity, ~65% relative humidity, 21ºC, 400 ppm [CO_2], and an air flow of 400 µmol s^{-1}. Stomatal conductance was recorded every 30 seconds for a total of 30 min. To control for the effect of the diurnal rhythm on stomatal physiology, gas exchange experiments began 2 hr after the beginning of the light cycle and measurements were made alternating between different genotypes. Data are presented as average stomatal conductance +/- standard error of 4 plants per genotype.

Fluorescence-activated nuclear sorting (FANS)
FANS was performed similar to (*36*) with small modifications. For experiments on seedlings, approximately 200 whole seedlings or whole roots severed with a scalpel were collected, transferred to a glass petri dish containing 2 ml of pre-chilled FANS-lysis buffer (15 mM Tris-HCl pH7.5, 20 mM NaCl, 80 mM KCl, 0.5 mM spermine, 1 mM spermidine, 5 mM 2-ME, 0.2% TritonX-100, 1 Pierce mini EDTA-free protease inhibitor cocktail), and chopped with a clean razor blade for 4 mins. Lysates were filtered through a 40 µm filter before transferring to new 15 ml tubes containing 4 ml of FANS-Sucrose buffer (20 mM Tris-HCl Ph8.0, 2 mM $MgCl_2$, 2 mM EDTAl, 15 mM 2-ME, 1.7 M sucrose, 0.2% TritonX-100). Nuclei were pelleted by centrifugation at 2200xg at 4C for 20 mins. The crude nuclei pellet was resuspended in 600 µl of FANS-lysis buffer supplemented with 4,6-Diamidino-2-phenylindole (DAPI).

For experiments on guard cells, the leaves of ~40 six-week-old plants were harvested and blended in 500 ml of ice-cold water for 2x30 secs with 1 min between pulses. The blended sample was then poured over a 100 µm mesh to remove mesophyll cells and collect epidermal enriched fragments. The mesh was gently rinsed with ~200 ml of water and after gently removing excess liquid, the thin sections of the collected epidermal tissue were flash-frozen in liquid nitrogen. Epidermal sections were ground in a frozen mortar and pestle to a fine powder.

After grinding, powder was transferred to a new mortar with a frozen metal. Immediately 12 ml of ice-cold FANS-lysis buffer was added, and the powder was gently resuspended with a clean pestle. The subsequent lysate was filtered through a 40 µm filter unit before transferring to a 15 ml tube containing 6 ml of FANS-Sucrose buffer. Nuclei were collected as above, before resuspending in 600 µl FANS-lysis buffer supplemented with DAPI.

Flow cytometry was conducted on a BD FACS Aria II using a 70 µm nozzle with a flow rate < 2 and the following photomultiplier tube parameters: FSC – 250 eV, SSC – 220 eV, BV421 – 550 eV, FITC – 340 eV. Sort gates were defined empirically to exclude debris and potential doublets. Before sorting GFP labeled nuclei, FACS analysis on unlabeled control samples was performed to define background signal. Sorted nuclei were collected in 600 µl of FANS-lysis buffer in a refrigerated tube chamber. Sort gates After sorting, nuclei were pelleted by centrifugation at 1000xg for 10 mins at 4C. Nuclei pellets were gently washed with 1 ml of 10 mM Tris-HCl pH8.0, 5 mM MgCl2 buffer, before centrifugation again as above. After carefully removing the supernatant, nuclei were used for ATAC-seq.

RNA-seq

For whole leaf RNA-seq, total RNA was extracted from the leaves from 6 plants per sample using the Spectrum total RNA isolation kit. For guard cell enriched RNA-seq, the leaves of 20 plants per sample were blended for 30 sec in ice-cold water, filtered through a 100 µm mesh, and then blended and filtered again as above to isolate epidermal tissue. Total RNA was then extracted using the Qiagen RNeasy mini kit. mRNA-seq libraries were prepared and sequenced on a NovaSeq 6000 (PE100) at the UCSD Institute for Genomic Medicine.

Following sequencing, adapter trimming and quality control checks were performed using Trim Galore version 0.6.5 (Cutadapt and FastQC). Reads were aligned to the Arabidopsis genome (TAIR10) by Rsubread version 2.14.0 (*79*). Low quality aligments (mapping quality < 2) were removed using Samtools view function version 1.17 (*80*). Read count per transcript matrices were generated using Rsubread featureCounts. Differential expression analysis was performed using DESeq2 version 1.26.0 (*81*). Transcripts were defined as significantly differentially expressed using the following thresholds: P adjusted value < 0.01 and fold change > 2. To visualize data using the Integrated Genome Browser (IGV), bigwig coverage tracks were generated using deepTools (version 3.5.0) bamCoverage function with a bin size of 1 bp and normalization using RPKM (*82*). Gene ontology (GO) term enrichment analysis was done using the Panther system (*83*).

ATAC-seq

ATAC-seq was performed as described in (*84*). Sorted nuclei were resuspended in 40 µl of tagmentation reaction mixture (20 µl 2xTD buffer, 0.4 µl 10% Tween, 0.4 µl 1% digitonin, 13.2 µl 1xPBS, X µl H2O) supplemented with TDE1 enzyme (Illumina) at a ratio of 2.0 µl TDE1:50,000 nuclei. Reactions were incubated at 37C for 30 mins. Tagmented DNA fragments were purified using the Qiagen min-Elute DNA kit. ATAC-seq libraries were amplified with dual indexed primers using the NEBNext 2xHiFi PCR Master Mix (New England Biolabs) for 5 initial cycles. The number of additional amplification cycles was determined empirically by performing qPCR on 10% of the amplified library. Amplified libraries dual size selected using a 0.6x-1.2X ratio of SPRIselect magnetic beads (Beckman Coulter). ATAC-seq libraries were pooled and sequenced on a NovaSeq 6000 (PE150 mode) by Novogene.

Following sequencing, adapter trimming and quality control checks were performed using Trim Galore version 0.6.5 (Cutadapt and FastQC). Parallel processing was performed using GNU Parallel (*85*). Reads were aligned to the Arabidopsis genome (TAIR10) by Rsubread version

2.14.0. Low quality aligments (mapping quality < 2) and alignments to the mitochondrial and chloroplast genomes were removed using Samtools view function version 1.17. Duplicated reads were filtered using Picard tools Markduplicates version 1.141. ATAC-seq peaks were called across all biological replicated using Genrich (*86*) with the following parameters: -r -d -j -p 0.01 -a 200. ATAC-seq peaks were then merged across all samples using bedtools merge function to generate a master list of peaks. ATAC-seq reads were then assigned to peaks using featureCounts and Fragments in peaks scores (FRiPs) were calucated. Differential chromatin accessibility analysis was performed using DESeq2 version 1.26.0. Regions were defined as significantly differentially accessible using the following thresholds: P adjusted value < 0.01 and fold change > 2. To visualize data using the Integrated Genome Browser (IGV), bigwig coverage tracks were generated on merged replicated bam files using deepTools (version 3.5.0) bamCoverage function with a bin size of 1 bp and normalization using RPKM. Peaks were assigned to nearest downstream gene (within 2 kb) by ChipSeeker (version 1.8.6) function seq2gene (*87*). Gene ontology (GO) term enrichment analysis was done using the Panther system. Heatmaps and metaplots of z score-normalized read depth were generated with DeepTools. Homer software (version 2.1.2) (*57*) was used to for de novo motif discovery for differentially accessible ATAC peaks and to match discovered motifs to previously known motifs from databases. We used ChIPpeakAnno software (Version 3.24) (*88*) to assign ATAC-seq peaks to annotated genomic features and to test for genomic overlap among different sets of peaks.

ACKNOWLEDGEMENTS

This research was supported by National Institutes of Health grant R01GM060396 to J.I.S. and by National Institutes of Health Ruth L. Kirschstein National Research Service Awards Postdoctoral Fellowship 5F32GM137544 to C.A.S. Experiments on CO2 responses were supported by National Science Foundation grant NSF MCB-1900567 to J.I.S. This publication includes data generated at the UC San Diego IGM Genomics Center utilizing an Illumina NovaSeq 6000 that was purchased with funding from a National Institutes of Health SIG grant (#S10 OD026929).

FIGURE LEGENDS

Figure 1. ABA induced rapid and genome-wide chromatin remodeling in seedlings. A) Volcano plot of differential ATACseq analysis showing regions that significantly change in chromatin accessibility in seedlings after 4hrs of ABA treatment. ABA increased accessibility at 638 regions and decreased accessibility at 372 regions (FDR < 0.01 and FC > 1.5). **B)** Heatmap of root nuclei ATAC-seq signal at regions showing ABA-regulated chromatin accessibility over the indicated ABA treatment time course. **C)** Number of ABA-regulated ATAC-seq peaks over time in roots. Bars summarizing ABA-induced peaks are colored in blue while bars representing ABA-repressed peaks are colored in pink. **D)** Genomic distribution among annotated features of all ATAC-seq peaks (orange) and in ABA-regulated ATAC-seq peaks (grey). **E)** Genome browser snapshots at three representative genes showing the change in ATAC-seq signal in upstream regions following ABA treatment. **F)** The transcription factor binding motifs with the highest enrichment in ABA-induced and ABA-repressed chromatin regions in roots.

Fig 2. Cell-type specific epigenomics identifies guard cell specific regulatory elements. A) Fluorescence micrograph showing guard cell specific expression of H2B-GFP. **B)** DAPI density plot shows that GFP positive nuclei (blue population) are diploid, while GFP negative nuclei (pink population) are distributed over multiple ploidies. **C)** FACS analysis of nuclei (DAPI positive) from *GC1:H2b-GFP* plants. GFP density plot defines two distinct populations

separated by GFP intensity. **D)** Chromatin accessibility heatmaps comparing ATAC-seq samples derived from guard cell, mesophyll, or root cell nuclei. ATAC-seq peaks are separated into guard cell specific (3272 ACRs), mesophyll specific(1472 ACRs), and root specific (3364 ACRs) sets defined by differential accessibility (p.adj < 0.001, FoldChange > 2). **E)** Principle component analysis (PCA) comparing ATAC-seq biological replicates derived from guard cell, mesophyll, or root nuclei. Samples clustered by tissue/cell-type of origin. **F)** ATAC-seq and RNA-seq metaplots showing average chromatin accessibility at guard cell specific peaks and average transcript levels of the nearest downstream gene (within 2 kb). Guard cell derived signal is shown in black while mesophyll/leaf signal is shown in green. **G)** Genome browser comparing ATAC-seq and RNA-seq signal for the indicated tracks at three example loci: two guard cell specific – *KAT1* and *SLAC1*, and one mesophyll cell specific gene – *AOC1*. **H)** Results of de novo motif analysis using homer. The top four most enriched motifs are shown along with the best matching known TFs and associated p-value.

Figure 3. ABA triggers extensive and persistent chromatin remodeling in guard cells. A) Schematic showing the experimental outline. Plants were sprayed with ABA and infrared images were taken using a thermal camera to assess stomatal closure. Guard cell nuclei were purified at 4hrs and 24 hrs after treatment and used for ATAC-seq. **B)** Volcano plot of guard cell enriched RNA-seq data showing ABA upregulates 2134 transcripts and downregulates 1452 transcripts. **C)** Heatmap of ATAC-seq signal in guard cell nuclei centered over 2260 regions with ABA-induced chromatin accessibility and 1662 regions with ABA-repressed chromatin accessibility (FDR < 0.001, FC > 2.0). **D)** Comparison of ABA-regulated peaks from 4hr and 24hr after treatment separated regions into three categories – early only, sustained (both early and late), and late only. The bar graph shows the number of ABA-increased and -decreased regions in each category. **E)** ATAC-seq and RNA-seq metaplots showing average chromatin accessibility and transcript levels near ABA-induced and ABA-repressed ATAC-seq peaks. **F,G)** Heatmap showing the results of homer motif analysis of ABA-increased **(F)** and ABA-decreased **(G)** ATAC-seq peaks. **H)** Genome browser images showing guard cell ATAC-seq and RNA-seq coverage at a representative ABA-induced gene (*DTX37)* and an ABA-repressed gene (*MYB60*). **I)** Overlap of ABA-induced accessible regions in guard cell nuclei, mesophyll nuclei, and root nuclei. **J)** Genome browser images showing guard cell ATAC-seq and RNA-seq coverage at *AKS3*. **K)** Fluorescence micrograph showing expression of *AKS3pr::GFP-AKS3* in guard cells after treatment with control or ABA (4 hr).

Fig 4. ABF transcription factors are required for ABA-induced chromatin opening in guard cells. A) Heatmap of ATAC-seq signal in either *WT* or *abfx4* mutant guard cells at 2029 regions with ABA-induced accessibility and 991 regions with ABA-repressed accessibility (FDR < 0.01 and FC > 2.0). **B)** Overlap of ABA-induced ATAC-seq peaks in *WT* guard cells with those in *abfx4* mutant guard cells. **C)** Genome browser snapshots showing ATAC-seq and RNA-seq signal near two ABA-induced genes *DTX37* and *HSGA6B*. **D)** Overlap between ABF DAP-seq peaks (Sun et al 2022) and ABA-induced accessible chromatin regions (ACRs). **E)** Peak metaplot showing ATAC-seq signal in the indicated samples at ABA-induced ATAC-seq peaks containing ABF DAP-seq binding sites. **F)** 1315 ABF-DAP-seq peaks overlapping ABA-induced ATAC-seq peaks or 1315 random ABF DAP-seq binding sites were assigned to nearest upstream genes. The plot shows the percentage of these genes that are transcriptionally induced by ABA treatment. **G)** Enrichment (-log P_value) of the indicated transcription factor binding motifs in ABA regulated ATAC-seq peaks in either *WT* or *abfx4* mutant guard cell nuclei. Negative enrichment scores indicate motifs overrepresented in condition-repressed regions. **H)** Bar plots representing the number of ABA-activated or ABA-repressed ACRs over time in *Col-0* or *abfx4* mutant roots.

Fig 5. ABA and changes in CO_2 concentration induce distinct chromatin remodeling programs in guard cells. A) Diagram showing the effects of different stimuli on the stomatal aperture. **B)** Representative IR image showing differences in leaf temperature due to CO_2 induced stomatal movement. **C-E)** Volcano plots of ATAC-seq data showing **C)** ABA-regulated chromatin accessibility, **D)** low CO_2 regulated chromatin accessibility, and **E)** high CO2 regulated chromatin accessibility. The number of differentially accessible peaks (colored in red, FDR < 0.01 and FC > 2.0) in each condition is indicated on each plot. **F)** Heatmaps of guard cell ATAC-seq signal centered over ABA-regulated ACRs (2029 induced and 991 repressed) and low CO_2-regulated ACRs (329 induced and 487 repressed). Libraries are derived from plants exposed to the indicated treatments. **G)** Principle component analysis (PCA) shows that ABA, low CO_2, and high CO_2 introduce separate variation to genome-wide chromatin accessibility. **H)** Genome browser snapshots showing ABA-repression of chromatin accessibility upstream of HT1, BLUS1, and CBC1 – three positive regulators of low CO_2 induced stomatal opening. **I)** Enrichment (-log P_value) of the indicated transcription factor binding motifs in ABA, Low CO2, or High CO_2 regulated regions. Negative enrichment scores indicate motifs overrepresented in condition-repressed regions.

Fig. 6 Model - ABA regulates opposing chromatin states in guard cells. In unstressed guard cells, AKS proteins maintain open chromatin at ABA-repressed genes while ABA-induced genes are kept silent by closed chromatin at their upstream regulatory regions. During abiotic stress, SnRK2s activate ABFs and inhibit AKSs. This leads to the establishment of open chromatin at stress-activated genes and the silencing of ABA-repressed genes by the closing of chromatin.

SUPPLEMENTAL CAPTIONS

Fig. S1. FANS-ATACseq on seedling nuclei reproducibly assays chromatin accessibility in regulatory DNA. A) Density plot DAPI fluorescence shows the distribution of ploidy among FACS-sorted nuclei from seedlings. **B)** Genome browser snapshot of a region of chromosome 1 showing ATACseq signal derived from either 50,000 seedling nuclei (two replicates shown in blue) or from purified genomic DNA (in pink). **C)** Open chromatin reads (<100 bp) of a seedling ATAC-seq library shows strong enrichment upstream of transcription start sites (TSSs). **D)** Scatterplot of ATAC-seq coverage showing correlation between two ATAC-seq replicates. **E)** Genomic distribution of seedling nuclei ATAC-seq peaks among annotated features.

Fig S2. Guard cell FANS-ATAC-seq. A) Diagram of the protocol used to isolate guard cell nuclei from *Arabidopsis* plants. The leaves of roughly 40 6-week-old GC1:H2b-GFP plants were blended in ice cold water. The resulting blendate was filtered through a 100 um mesh sheet to isolate epidermal tissue. A representative fluorescence micrograph shows intact guard cells with nuclei labeled by H2b-GFP. Epidermal tissue was flash frozen in LN2 and then ground to a fine powder using a mortar and pestle. After extracting nuclei from ground tissue, GFP positive nuclei were purified using FACS. **B)** DAPI vs GFP intensity plot resulting from FACS analysis of nuclei (DAPI positive) from *GC1:H2b-GFP* plants (in green) and *Col-0* plants (in black). **C)** Sorted guard cell nuclei were re-run through the same FACS protocol to evaluate the purity of the isolated population. The DAPI vs GFP plot shows nuclei passing (green) and failing (black) the sorting criteria. Out of 10,000 sorted nuclei, 9821 passed (purity of 98%). **D)** Pie chart displaying the distribution of guard cell ATAC-seq peaks among annotated genomic features are colored in green while nuclei that failed GFP density plot defines two distinct populations separated by GFP intensity. **E)** TSS enrichment plot showing open chromatin reads (<100 bp) of a Guard Cell ATAC-seq library shows strong enrichment upstream of transcription start sites

(TSSs). **F)** Scatterplots showing the correlation among biological replicates of guard cell ATAC-seq libraries.

Figure S3. ABA induced chromatin remodeling in mesophyll cell nuclei. A) GFP vs DAPI intensity plot showing the results of FACS analysis on nuclei from *RBCp::H2b-GFP* plants. The location of GFP positive mesophyll nuclei sorted for ATAC-seq is indicated dashed box. Inset shows a confocal image showing the expression of *RBCp::H2b-GFP* in mesophyll cell nuclei. **B)** ATAC-seq coverage plot showing strong enrichment of mesophyll ATAC-seq reads upstream of Transcription Start Sites (TSSs). **F)** Representative IF image showing increase in leaf surface temperature 3hrs after spraying *RBC:H2b-GFP* plants with ABA. **D)** Heatmap of ATAC-seq signal in mesophyll nuclei at regions showing ABA-regulated chromatin accessibility. ABA significantly increased accessibility at 926 regions and decreased accessibility at 436 regions (FDR < 0.01 and FC > 1.5). **E)** Genome browser snapshots at representative genes (*MAPKKK18* and HB12) showing ABA-regulated chromatin accessibility in upstream sequences. **F)** Selection of transcription factor binding motifs enriched in ABA-induced and ABA-repressed ATAC-seq regions in mesophyll nuclei.

Fig S4. RNA-seq identifies ABA-regulated transcripts in guard cells and wholeleaf tissue. A) Volcano plot of differential RNA-seq analysis (FDR < 0.001, FC > 2) comparing control and ABA-treated samples from both whole leaf and guard cells. Differentially expressed transcripts are colored in red (2316 upregulated and 1529 downregulated). **B)** Principle component analysis (PCA) of RNA-seq results showing samples clustering by treatment (ABA vs control) and cell-type (guard cell vs leaf). **C)** Overlap of transcripts induced or repressed by ABA between whole leaves and guard cells. **D)** Results of a Gene Ontology (GO) analysis performed on ABA-induced transcripts. **E)** Genome browser snapshots showing RNA-seq signal from the indicated samples at the representative ABA-regulated genes *HAI2, AT2G37900,* and *AAE9*.

Fig. S5. ABA triggered chromatin remodeling in guard cells. A) PCA plot of guard cell ATAC-seq samples from ABA treatment experiment. **B)** De novo motif discovery uncovered motifs similar to ABF1 and AKS3 in ABA-activated and ABA-repressed ACRs, respectively. Metaplots of control and ABA-treated guard cell ATAC-seq samples centered over peaks containing either of these motifs are shown below the indicated DNA motifs. **C)** Genomic distribution among annotated features of guard cell ATAC-seq peaks separated into regions that are static (black) and those that are ABA-regulated (orange).

Fig. S6. Examples of ABA triggered chromatin remodeling in guard cells. Additional examples of ABA-induced changes to chromatin accessibility upstream of known regulators of stomatal movements including **A)** *MYB21*, **B)** *NCED3*, **C)** *HT1*, and additional genes of interest including **D)** the wax biosynthesis gene *AAE9*, **E)** *RD29B*, **F)** the aquaporin *PIP1;4*, **G)** *LTP4*, and **H)** the cell wall expansin *EXPA1*.

Fig S7. The ABRE binding proteins ABF1-4 are required for the bulk of ABA-induced transcription in mature leaf tissue. A) Volcano plot of RNA-seq results from ABA or control treated 5-week old *abfx4* mutant leaf tissue. ABA signigicantly upregulated 561 transcripts and downregulated 724 transcripts (FDR < 0.01 and FC > 2). **B)** Overlap of ABA-induced transcripts in *Col-0* leaves vs *abfx4* mutant leaves shows that ABFs are required for the upregulation of 2030 transcripts. **C)** Genome browser snapshots showing guard cell ATAC-seq signal and RNA-seq signal 4 genes encoding ABFs. Chromatin accessibility upstream of *ABF1-4* was not significantly increased by ABA in guard cells. **D)** Gas exchange (Licor-6400) comparing steady state stomatal conductance of well-watered Col-0 and abfx4 plants (n = 5 per genotype).

Fig S8. Chromatin accessibility in *abfx4* mutant guard cells without ABA treatment. A) Confocal image showing guard cell specific expression of H2B-GFP in *abfx4* mutant leaf. **B)** Principle component analysis (PCA) of Guard cell ATAC-seq results showing samples clustering by treatment (ABA vs control) and genotype (*Col-0* vs *abfx4*). **C)** Volcano plot summarizing differential ATAC-seq analysis (FDR < 0.01 and FC > 2.0) comparing chromatin accessibility in control treated *WT* vs *abfx4* mutant guard cells.

Fig S9. ABFs are required for ABA-induced chromatin opening in roots. A) Heatmap of ATAC-seq signal at regions showing ABA-regulated chromatin accessibility over the indicated ABA treatment time course in either *WT* or *abfx4* mutant root nuclei. **B)** Principle component analysis of root ATAC-seq libraries showing separation of samples by both genotype and ABA treatment duration. **C)** Genome browser snapshot showing chromatin accessibility in *WT* or *abfx4* mutant root nuclei upstream of the ABA-induced gene *MAPKKK18* over the indicated ABA treatment time series.

Fig S10. Distinct regulation of chromatin by ABA and CO_2 in guard cells. A) UpSet plot showing the set relationships between ABA, low CO_2, and high CO^2 regulated ATAC-seq peaks. Overlapping sets are indicated by the filled in circles below the bar graph and the number of peaks contained within the set is labeled above the respective bar. **B-E)** Genome browser images showing ABA and CO_2-regulated chromatin accessibility upstream of **B)** *ERF113*, **C)** *AT2G25070*, **D)** *ALMT6*, and **E)** *CBP60F*.

REFERENCES

1. R. J. Schmitz, E. Grotewold, M. Stam, Cis-regulatory sequences in plants: Their importance, discovery, and future challenges. *The Plant Cell*. **34**, 718–741 (2022).

2. W. K. M. Lai, B. F. Pugh, Understanding nucleosome dynamics and their links to gene expression and DNA replication. *Nature Reviews Molecular Cell Biology*. **18**, 548–562 (2017).

3. T. C. Voss, G. L. Hager, Dynamic regulation of transcriptional states by chromatin and transcription factors. *Nature Reviews Genetics*. **15**, 69–81 (2014).

4. J. L. Nemhauser, F. Hong, J. Chory, Different Plant Hormones Regulate Similar Processes through Largely Nonoverlapping Transcriptional Responses. *Cell*. **126**, 467–475 (2006).

5. R. Waadt, C. A. Seller, P.-K. Hsu, Y. Takahashi, S. Munemasa, J. I. Schroeder, Plant hormone regulation of abiotic stress responses. *Nat Rev Mol Cell Biol*. **23**, 680–694 (2022).

6. P. Sijacic, M. Bajic, E. C. McKinney, R. B. Meagher, R. B. Deal, Changes in chromatin accessibility between Arabidopsis stem cells and mesophyll cells illuminate cell type-specific transcription factor networks. *The Plant Journal*. **94**, 215–231 (2018).

7. K. A. Maher, M. Bajic, K. Kajala, M. Reynoso, G. Pauluzzi, D. A. West, K. Zumstein, M. Woodhouse, K. Bubb, M. W. Dorrity, C. Queitsch, J. Bailey-Serres, N. Sinha, S. M. Brady, R. B. Deal, Profiling of Accessible Chromatin Regions across Multiple Plant Species and

Cell Types Reveals Common Gene Regulatory Principles and New Control Modules. *The Plant Cell*. **30**, 15–36 (2018).

8. A. Farmer, S. Thibivilliers, K. H. Ryu, J. Schiefelbein, M. Libault, Single-nucleus RNA and ATAC sequencing reveals the impact of chromatin accessibility on gene expression in Arabidopsis roots at the single-cell level. *Molecular Plant*. **14**, 372–383 (2021).

9. M. Borg, R. K. Papareddy, R. Dombey, E. Axelsson, M. D. Nodine, D. Twell, F. Berger, Epigenetic reprogramming rewires transcription during the alternation of generations in Arabidopsis. *eLife*. **10**, e61894 (2021).

10. A. P. Marand, Z. Chen, A. Gallavotti, R. J. Schmitz, A cis-regulatory atlas in maize at single-cell resolution. *Cell*. **184**, 3041-3055.e21 (2021).

11. E.-D. Kim, M. W. Dorrity, B. A. Fitzgerald, H. Seo, K. M. Sepuru, C. Queitsch, N. Mitsuda, S.-K. Han, K. U. Torii, Dynamic chromatin accessibility deploys heterotypic cis/trans-acting factors driving stomatal cell-fate commitment. *Nat. Plants*. **8**, 1453–1466 (2022).

12. S. R. Cutler, P. L. Rodriguez, R. R. Finkelstein, S. R. Abrams, Abscisic Acid: Emergence of a Core Signaling Network. *Annual Review of Plant Biology*. **61**, 651–679 (2010).

13. R. Finkelstein, Abscisic Acid Synthesis and Response. *Arabidopsis Book*. **11** (2013), doi:10.1199/tab.0166.

14. J.-K. Zhu, Abiotic Stress Signaling and Responses in Plants. *Cell*. **167**, 313–324 (2016).

15. Y. Ma, I. Szostkiewicz, A. Korte, D. Moes, Y. Yang, A. Christmann, E. Grill, Regulators of PP2C Phosphatase Activity Function as Abscisic Acid Sensors. *Science*. **324**, 1064–1068 (2009).

16. S.-Y. Park, P. Fung, N. Nishimura, D. R. Jensen, H. Fujii, Y. Zhao, S. Lumba, J. Santiago, A. Rodrigues, T. F. Chow, S. E. Alfred, D. Bonetta, R. Finkelstein, N. J. Provart, D. Desveaux, P. L. Rodriguez, P. McCourt, J.-K. Zhu, J. I. Schroeder, B. F. Volkman, S. R. Cutler, Abscisic Acid Inhibits Type 2C Protein Phosphatases via the PYR/PYL Family of START Proteins. *Science*. **324**, 1068–1071 (2009).

17. T. Umezawa, N. Sugiyama, M. Mizoguchi, S. Hayashi, F. Myouga, K. Yamaguchi-Shinozaki, Y. Ishihama, T. Hirayama, K. Shinozaki, Type 2C protein phosphatases directly regulate abscisic acid-activated protein kinases in Arabidopsis. *Proceedings of the National Academy of Sciences*. **106**, 17588–17593 (2009).

18. H. Fujii, P. E. Verslues, J.-K. Zhu, Identification of Two Protein Kinases Required for Abscisic Acid Regulation of Seed Germination, Root Growth, and Gene Expression in Arabidopsis. *The Plant Cell*. **19**, 485–494 (2007).

19. K. E. Hubbard, N. Nishimura, K. Hitomi, E. D. Getzoff, J. I. Schroeder, Early abscisic acid signal transduction mechanisms: newly discovered components and newly emerging questions. *Genes Dev.* **24**, 1695–1708 (2010).

20. Y. Takahashi, Y. Ebisu, T. Kinoshita, M. Doi, E. Okuma, Y. Murata, K. Shimazaki, bHLH Transcription Factors That Facilitate K+ Uptake During Stomatal Opening Are Repressed by Abscisic Acid Through Phosphorylation. *Science Signaling*. **6**, ra48–ra48 (2013).

21. T. Yoshida, Y. Fujita, H. Sayama, S. Kidokoro, K. Maruyama, J. Mizoi, K. Shinozaki, K. Yamaguchi-Shinozaki, AREB1, AREB2, and ABF3 are master transcription factors that cooperatively regulate ABRE-dependent ABA signaling involved in drought stress tolerance and require ABA for full activation. *The Plant Journal*. **61**, 672–685 (2010).

22. T. Yoshida, Y. Fujita, K. Maruyama, J. Mogami, D. Todaka, K. Shinozaki, K. Yamaguchi-Shinozaki, Four Arabidopsis AREB/ABF transcription factors function predominantly in gene expression downstream of SnRK2 kinases in abscisic acid signalling in response to osmotic stress. *Plant, Cell & Environment*. **38**, 35–49 (2015).

23. P. Wang, L. Xue, G. Batelli, S. Lee, Y.-J. Hou, M. J. V. Oosten, H. Zhang, W. A. Tao, J.-K. Zhu, Quantitative phosphoproteomics identifies SnRK2 protein kinase substrates and reveals the effectors of abscisic acid action. *PNAS*. **110**, 11205–11210 (2013).

24. T. Umezawa, N. Sugiyama, F. Takahashi, J. C. Anderson, Y. Ishihama, S. C. Peck, K. Shinozaki, Genetics and Phosphoproteomics Reveal a Protein Phosphorylation Network in the Abscisic Acid Signaling Pathway in Arabidopsis thaliana. *Sci. Signal.* **6**, rs8–rs8 (2013).

25. N. Leonhardt, J. M. Kwak, N. Robert, D. Waner, G. Leonhardt, J. I. Schroeder, Microarray Expression Analyses of Arabidopsis Guard Cells and Isolation of a Recessive Abscisic Acid Hypersensitive Protein Phosphatase 2C Mutant. *The Plant Cell*. **16**, 596–615 (2004).

26. H. Goda, E. Sasaki, K. Akiyama, A. Maruyama-Nakashita, K. Nakabayashi, W. Li, M. Ogawa, Y. Yamauchi, J. Preston, K. Aoki, T. Kiba, S. Takatsuto, S. Fujioka, T. Asami, T. Nakano, H. Kato, T. Mizuno, H. Sakakibara, S. Yamaguchi, E. Nambara, Y. Kamiya, H. Takahashi, M. Y. Hirai, T. Sakurai, K. Shinozaki, K. Saito, S. Yoshida, Y. Shimada, The AtGenExpress hormone and chemical treatment data set: experimental design, data evaluation, model data analysis and data access. *The Plant Journal*. **55**, 526–542 (2008).

27. R.-S. Wang, S. Pandey, S. Li, T. E. Gookin, Z. Zhao, R. Albert, S. M. Assmann, Common and unique elements of the ABA-regulated transcriptome of Arabidopsis guard cells. *BMC Genomics*. **12**, 216 (2011).

28. A. M. Hetherington, F. I. Woodward, The role of stomata in sensing and driving environmental change. *Nature*. **424**, 901–908 (2003).

29. S. M. Assmann, T. Jegla, Guard cell sensory systems: recent insights on stomatal responses to light, abscisic acid, and CO2. *Current Opinion in Plant Biology*. **33**, 157–167 (2016).

30. G. Dubeaux, P.-K. Hsu, P. H. O. Ceciliato, K. J. Swink, W.-J. Rappel, J. I. Schroeder, Deep dive into CO2-dependent molecular mechanisms driving stomatal responses in plants. *Plant Physiology*. **187**, 2032–2042 (2021).

31. Z. Liu, Y. Zhou, J. Guo, J. Li, Z. Tian, Z. Zhu, J. Wang, R. Wu, B. Zhang, Y. Hu, Y. Sun, Y. Shangguan, W. Li, T. Li, Y. Hu, C. Guo, J.-D. Rochaix, Y. Miao, X. Sun, Global Dynamic

Molecular Profiling of Stomatal Lineage Cell Development by Single-Cell RNA Sequencing. *Molecular Plant*. **13**, 1178–1193 (2020).

32. C. B. Lopez-Anido, A. Vatén, N. K. Smoot, N. Sharma, V. Guo, Y. Gong, M. X. Anleu Gil, A. K. Weimer, D. C. Bergmann, Single-cell resolution of lineage trajectories in the Arabidopsis stomatal lineage and developing leaf. *Developmental Cell*. **56**, 1043-1055.e4 (2021).

33. J.-Y. Kim, E. Symeonidi, T. Y. Pang, T. Denyer, D. Weidauer, M. Bezrutczyk, M. Miras, N. Zöllner, T. Hartwig, M. M. Wudick, M. Lercher, L.-Q. Chen, M. C. P. Timmermans, W. B. Frommer, Distinct identities of leaf phloem cells revealed by single cell transcriptomics. *The Plant Cell*. **33**, 511–530 (2021).

34. C. Procko, T. Lee, A. Borsuk, B. O. R. Bargmann, T. Dabi, J. R. Nery, M. Estelle, L. Baird, C. O'Connor, C. Brodersen, J. R. Ecker, J. Chory, Leaf cell-specific and single-cell transcriptional profiling reveals a role for the palisade layer in UV light protection. *The Plant Cell*. **34**, 3261–3279 (2022).

35. J. D. Buenrostro, P. G. Giresi, L. C. Zaba, H. Y. Chang, W. J. Greenleaf, Transposition of native chromatin for fast and sensitive epigenomic profiling of open chromatin, DNA-binding proteins and nucleosome position. *Nature Methods*. **10**, 1213–1218 (2013).

36. Z. Lu, B. T. Hofmeister, C. Vollmers, R. M. DuBois, R. J. Schmitz, Combining ATAC-seq with nuclei sorting for discovery of cis-regulatory regions in plant genomes. *Nucleic Acids Research*. **45**, e41 (2017).

37. A. M. Jones, J. Å. Danielson, S. N. ManojKumar, V. Lanquar, G. Grossmann, W. B. Frommer, Abscisic acid dynamics in roots detected with genetically encoded FRET sensors. *eLife*. **3**, e01741 (2014).

38. R. Waadt, K. Hitomi, N. Nishimura, C. Hitomi, S. R. Adams, E. D. Getzoff, J. I. Schroeder, FRET-based reporters for the direct visualization of abscisic acid concentration changes and distribution in Arabidopsis. *eLife*. **3**, e01739 (2014).

39. R. C. O'Malley, S. C. Huang, L. Song, M. G. Lewsey, A. Bartlett, J. R. Nery, M. Galli, A. Gallavotti, J. R. Ecker, Cistrome and Epicistrome Features Shape the Regulatory DNA Landscape. *Cell*. **165**, 1280–1292 (2016).

40. Y. Takahashi, T. Kinoshita, M. Matsumoto, K. Shimazaki, Inhibition of the Arabidopsis bHLH transcription factor by monomerization through abscisic acid-induced phosphorylation. *The Plant Journal*. **87**, 559–567 (2016).

41. Y. Yang, A. Costa, N. Leonhardt, R. S. Siegel, J. I. Schroeder, Isolation of a strong Arabidopsis guard cell promoter and its potential as a research tool. *Plant Methods*. **4**, 6 (2008).

42. M. M. Marquès-Bueno, A. K. Morao, A. Cayrel, M. P. Platre, M. Barberon, E. Caillieux, V. Colot, Y. Jaillais, F. Roudier, G. Vert, A versatile Multisite Gateway-compatible promoter and transgenic line collection for cell type-specific functional genomics in Arabidopsis. *The Plant Journal*. **85**, 320–333 (2016).

43. J. A. Anderson, S. S. Huprikar, L. V. Kochian, W. J. Lucas, R. F. Gaber, Functional expression of a probable Arabidopsis thaliana potassium channel in Saccharomyces cerevisiae. *Proceedings of the National Academy of Sciences*. **89**, 3736–3740 (1992).

44. D. P. Schachtman, J. 1. Schroeder, W. J. Lucas, J. A. Anderson, R. F. Gaber, Expression of an Inward-Rectifying Potassium Channel by the Arabidopsis KAT1 cDNA. *Science*. **258**, 1654–1658 (1992).

45. R. L. Nakamura, W. L. McKendree Jr, R. E. Hirsch, J. C. Sedbrook, R. F. Gaber, M. R. Sussman, Expression of an Arabidopsis Potassium Channel Gene in Guard Cells. *Plant Physiology*. **109**, 371–374 (1995).

46. J. Negi, O. Matsuda, T. Nagasawa, Y. Oba, H. Takahashi, M. Kawai-Yamada, H. Uchimiya, M. Hashimoto, K. Iba, CO2 regulator SLAC1 and its homologues are essential for anion homeostasis in plant cells. *Nature*. **452**, 483–486 (2008).

47. T. Vahisalu, H. Kollist, Y.-F. Wang, N. Nishimura, W.-Y. Chan, G. Valerio, A. Lamminmäki, M. Brosché, H. Moldau, R. Desikan, J. I. Schroeder, J. Kangasjärvi, SLAC1 is required for plant guard cell S-type anion channel function in stomatal signalling. *Nature*. **452**, 487–491 (2008).

48. K. Ohashi-Ito, D. C. Bergmann, Arabidopsis FAMA Controls the Final Proliferation/Differentiation Switch during Stomatal Development. *The Plant Cell*. **18**, 2493–2505 (2006).

49. J. Negi, K. Moriwaki, M. Konishi, R. Yokoyama, T. Nakano, K. Kusumi, M. Hashimoto-Sugimoto, J. I. Schroeder, K. Nishitani, S. Yanagisawa, K. Iba, A Dof Transcription Factor, SCAP1, Is Essential for the Development of Functional Stomata in Arabidopsis. *Current Biology*. **23**, 479–484 (2013).

50. S. Li, X. Yang, H. Huang, R. Qiao, M. A. Jenks, H. Zhao, S. Lü, Arabidopsis ACYL-ACTIVATING ENZYME 9 (AAE9) encoding an isobutyl-CoA synthetase is a key factor connecting branched-chain amino acid catabolism with iso-branched wax biosynthesis. *New Phytologist*. **233**, 2458–2470 (2022).

51. Y.-K. Liang, C. Dubos, I. C. Dodd, G. H. Holroyd, A. M. Hetherington, M. M. Campbell, AtMYB61, an R2R3-MYB Transcription Factor Controlling Stomatal Aperture in Arabidopsis thaliana. *Current Biology*. **15**, 1201–1206 (2005).

52. M. B. Prouse, M. M. Campbell, Interactions between the R2R3-MYB Transcription Factor, AtMYB61, and Target DNA Binding Sites. *PLOS ONE*. **8**, e65132 (2013).

53. S. J. Gilmour, D. G. Zarka, E. J. Stockinger, M. P. Salazar, J. M. Houghton, M. F. Thomashow, Low temperature regulation of the Arabidopsis CBF family of AP2 transcriptional activators as an early step in cold-induced COR gene expression. *The Plant Journal*. **16**, 433–442 (1998).

54. E. Cominelli, M. Galbiati, A. Vavasseur, L. Conti, T. Sala, M. Vuylsteke, N. Leonhardt, S. L. Dellaporta, C. Tonelli, A Guard-Cell-Specific MYB Transcription Factor Regulates Stomatal Movements and Plant Drought Tolerance. *Current Biology*. **15**, 1196–1200 (2005).

55. M. Hashimoto, J. Negi, J. Young, M. Israelsson, J. I. Schroeder, K. Iba, Arabidopsis HT1 kinase controls stomatal movements in response to CO2. *Nat Cell Biol*. **8**, 391–397 (2006).

56. Y. Sun, D.-H. Oh, L. Duan, P. Ramachandran, A. Ramirez, A. Bartlett, K.-N. Tran, G. Wang, M. Dassanayake, J. R. Dinneny, Divergence in the ABA gene regulatory network underlies differential growth control. *Nat. Plants*, 1–12 (2022).

57. S. Heinz, C. Benner, N. Spann, E. Bertolino, Y. C. Lin, P. Laslo, J. X. Cheng, C. Murre, H. Singh, C. K. Glass, Simple Combinations of Lineage-Determining Transcription Factors Prime cis-Regulatory Elements Required for Macrophage and B Cell Identities. *Molecular Cell*. **38**, 576–589 (2010).

58. W. Lahr, K. Raschke, Abscisic-acid contents and concentrations in protoplasts from guard cells and mesophyll cells ofVicia faba L. *Planta*. **173**, 528–531 (1988).

59. P.-K. Hsu, Y. Takahashi, S. Munemasa, E. Merilo, K. Laanemets, R. Waadt, D. Pater, H. Kollist, J. I. Schroeder, Abscisic acid-independent stomatal CO2 signal transduction pathway and convergence of CO2 and ABA signaling downstream of OST1 kinase. *Proceedings of the National Academy of Sciences*. **115**, E9971–E9980 (2018).

60. M. Dittrich, H. M. Mueller, H. Bauer, M. Peirats-Llobet, P. L. Rodriguez, C.-M. Geilfus, S. C. Carpentier, K. A. S. Al Rasheid, H. Kollist, E. Merilo, J. Herrmann, T. Müller, P. Ache, A. M. Hetherington, R. Hedrich, The role of Arabidopsis ABA receptors from the PYR/PYL/RCAR family in stomatal acclimation and closure signal integration. *Nat. Plants*. **5**, 1002–1011 (2019).

61. L. Zhang, Y. Takahashi, P.-K. Hsu, H. Kollist, E. Merilo, P. J. Krysan, J. I. Schroeder, FRET kinase sensor development reveals SnRK2/OST1 activation by ABA but not by MeJA and high CO2 during stomatal closure. *eLife*. **9**, e56351 (2020).

62. A. Hiyama, A. Takemiya, S. Munemasa, E. Okuma, N. Sugiyama, Y. Tada, Y. Murata, K. Shimazaki, Blue light and CO2 signals converge to regulate light-induced stomatal opening. *Nat Commun*. **8**, 1284 (2017).

63. K. C. Potter, J. Wang, G. E. Schaller, J. J. Kieber, Cytokinin modulates context-dependent chromatin accessibility through the type-B response regulators. *Nature Plants*. **4**, 1102–1111 (2018).

64. M. Iwafuchi-Doi, K. S. Zaret, Pioneer transcription factors in cell reprogramming. *Genes Dev.* **28**, 2679–2692 (2014).

65. A. Balsalobre, J. Drouin, Pioneer factors as master regulators of the epigenome and cell fate. *Nat Rev Mol Cell Biol*, 1–16 (2022).

66. R. Jin, S. Klasfeld, Y. Zhu, M. Fernandez Garcia, J. Xiao, S.-K. Han, A. Konkol, D. Wagner, LEAFY is a pioneer transcription factor and licenses cell reprogramming to floral fate. *Nat Commun*. **12**, 626 (2021).

67. C. van Oevelen, S. Collombet, G. Vicent, M. Hoogenkamp, C. Lepoivre, A. Badeaux, L. Bussmann, J. L. Sardina, D. Thieffry, M. Beato, Y. Shi, C. Bonifer, T. Graf, C/EBPα

Activates Pre-existing and De Novo Macrophage Enhancers during Induced Pre-B Cell Transdifferentiation and Myelopoiesis. *Stem Cell Reports*. **5**, 232–247 (2015).

68. S.-K. Han, Y. Sang, A. Rodrigues, B. F2010, M.-F. Wu, P. L. Rodriguez, D. Wagner, The SWI2/SNF2 Chromatin Remodeling ATPase BRAHMA Represses Abscisic Acid Responses in the Absence of the Stress Stimulus in Arabidopsis. *The Plant Cell*. **24**, 4892–4906 (2012).

69. M. Peirats-Llobet, S.-K. Han, M. Gonzalez-Guzman, C. W. Jeong, L. Rodriguez, B. Belda-Palazon, D. Wagner, P. L. Rodriguez, A Direct Link between Abscisic Acid Sensing and the Chromatin-Remodeling ATPase BRAHMA via Core ABA Signaling Pathway Components. *Molecular Plant*. **9**, 136–147 (2016).

70. D. Baek, G. Shin, M. C. Kim, M. Shen, S. Y. Lee, D.-J. Yun, Histone Deacetylase HDA9 With ABI4 Contributes to Abscisic Acid Homeostasis in Drought Stress Response. *Frontiers in Plant Science*. **11** (2020) (available at https://www.frontiersin.org/articles/10.3389/fpls.2020.00143).

71. R. Finkelstein, S. S. L. Gampala, T. J. Lynch, T. L. Thomas, C. D. Rock, Redundant and Distinct Functions of the ABA Response Loci ABA-INSENSITIVE(ABI)5 and ABRE-BINDING FACTOR (ABF)3. *Plant Mol Biol*. **59**, 253–267 (2005).

72. R. R. Finkelstein, T. J. Lynch, The Arabidopsis Abscisic Acid Response Gene ABI5 Encodes a Basic Leucine Zipper Transcription Factor. *The Plant Cell*. **12**, 599–609 (2000).

73. E. Fleta-Soriano, M. Pintó-Marijuan, S. Munné-Bosch, Evidence of Drought Stress Memory in the Facultative CAM, Aptenia cordifolia: Possible Role of Phytohormones. *PLOS ONE*. **10**, e0135391 (2015).

74. P. A. Auler, F. B. S. Freire, V. F. Lima, D. M. Daloso, On the role of guard cells in sensing environmental signals and memorising stress periods. *Theor. Exp. Plant Physiol.* **34**, 277–299 (2022).

75. Y. Ding, M. Fromm, Z. Avramova, Multiple exposures to drought “train” transcriptional responses in *Arabidopsis*. *Nature Communications*. **3**, 740 (2012).

76. L. Virlouvet, M. Fromm, Physiological and transcriptional memory in guard cells during repetitive dehydration stress. *New Phytologist*. **205**, 596–607 (2015).

77. A. van Weringh, A. Pasha, E. Esteban, P. J. Gamueda, N. J. Provart, Generation of guard cell RNA-seq transcriptomes during progressive drought and recovery using an adapted INTACT protocol for Arabidopsis thaliana shoot tissue (2021), p. 2021.04.15.439991, , doi:10.1101/2021.04.15.439991.

78. A. Lampropoulos, Z. Sutikovic, C. Wenzl, I. Maegele, J. U. Lohmann, J. Forner, GreenGate - A Novel, Versatile, and Efficient Cloning System for Plant Transgenesis. *PLOS ONE*. **8**, e83043 (2013).

79. Y. Liao, G. K. Smyth, W. Shi, The R package Rsubread is easier, faster, cheaper and better for alignment and quantification of RNA sequencing reads. *Nucleic Acids Research*. **47**, e47 (2019).

80. H. Li, B. Handsaker, A. Wysoker, T. Fennell, J. Ruan, N. Homer, G. Marth, G. Abecasis, R. Durbin, 1000 Genome Project Data Processing Subgroup, The Sequence Alignment/Map format and SAMtools. *Bioinformatics*. **25**, 2078–2079 (2009).

81. M. I. Love, W. Huber, S. Anders, Moderated estimation of fold change and dispersion for RNA-seq data with DESeq2. *Genome Biology*. **15**, 550 (2014).

82. F. Ramírez, D. P. Ryan, B. Grüning, V. Bhardwaj, F. Kilpert, A. S. Richter, S. Heyne, F. Dündar, T. Manke, deepTools2: a next generation web server for deep-sequencing data analysis. *Nucleic Acids Research*. **44**, W160–W165 (2016).

83. H. Mi, A. Muruganujan, D. Ebert, X. Huang, P. D. Thomas, PANTHER version 14: more genomes, a new PANTHER GO-slim and improvements in enrichment analysis tools. *Nucleic Acids Research*. **47**, D419–D426 (2019).

84. J. Buenrostro, B. Wu, H. Chang, W. Greenleaf, *Curr Protoc Mol Biol*, in press, doi:10.1002/0471142727.mb2129s109.

85. O. Tange, GNU Parallel 20220922 ('Elizabeth'). *Zenodo* (2022), doi:10.5281/zenodo.7105792.

86. J. M. Gaspar, Genrich: detecting sites of genomic enrichment (2021), (available at https://github.com/jsh58/Genrich#readme).

87. G. Yu, L.-G. Wang, Q.-Y. He, ChIPseeker: an R/Bioconductor package for ChIP peak annotation, comparison and visualization. *Bioinformatics*. **31**, 2382–2383 (2015).

88. L. J. Zhu, C. Gazin, N. D. Lawson, H. Pagès, S. M. Lin, D. S. Lapointe, M. R. Green, ChIPpeakAnno: a Bioconductor package to annotate ChIP-seq and ChIP-chip data. *BMC Bioinformatics*. **11**, 237 (2010).

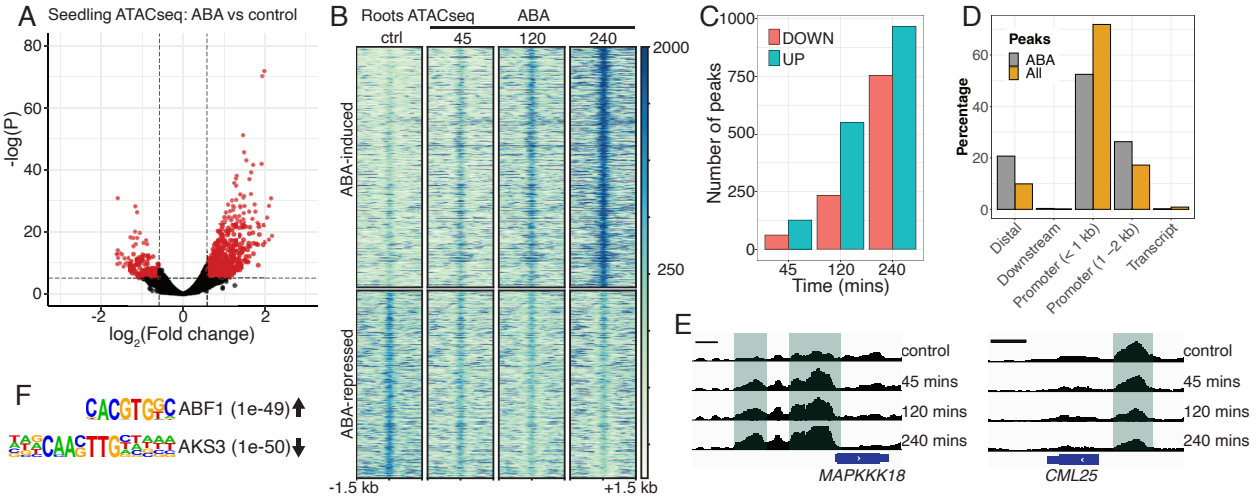

Figure 1. ABA induced rapid and genome-wide chromatin remodeling in seedlings. A) Volcano plot of differential ATACseq analysis showing regions that significantly change in chromatin accessibility in seedlings after 4hrs of ABA treatment. ABA increased accessibility at 638 regions and decreased accessibility at 372 regions (FDR < 0.01 and FC > 1.5). **B)** Heatmap of root nuclei ATAC-seq signal at regions showing ABA-regulated chromatin accessibility over the indicated ABA treatment time course. **C)** Number of ABA-regulated ATAC-seq peaks over time in roots. Bars summarizing ABA-induced peaks are colored in blue while bars representing ABA-repressed peaks are colored in pink. **D)** Genomic distribution among annotated features of all ATAC-seq peaks (orange) and in ABA-regulated ATAC-seq peaks (grey). **E)** Genome browser snapshots at three representative genes showing the change in ATAC-seq signal in upstream regions following ABA treatment. **F)** The transcription factor binding motifs with the highest enrichment in ABA-induced and ABA-repressed chromatin regions in roots.

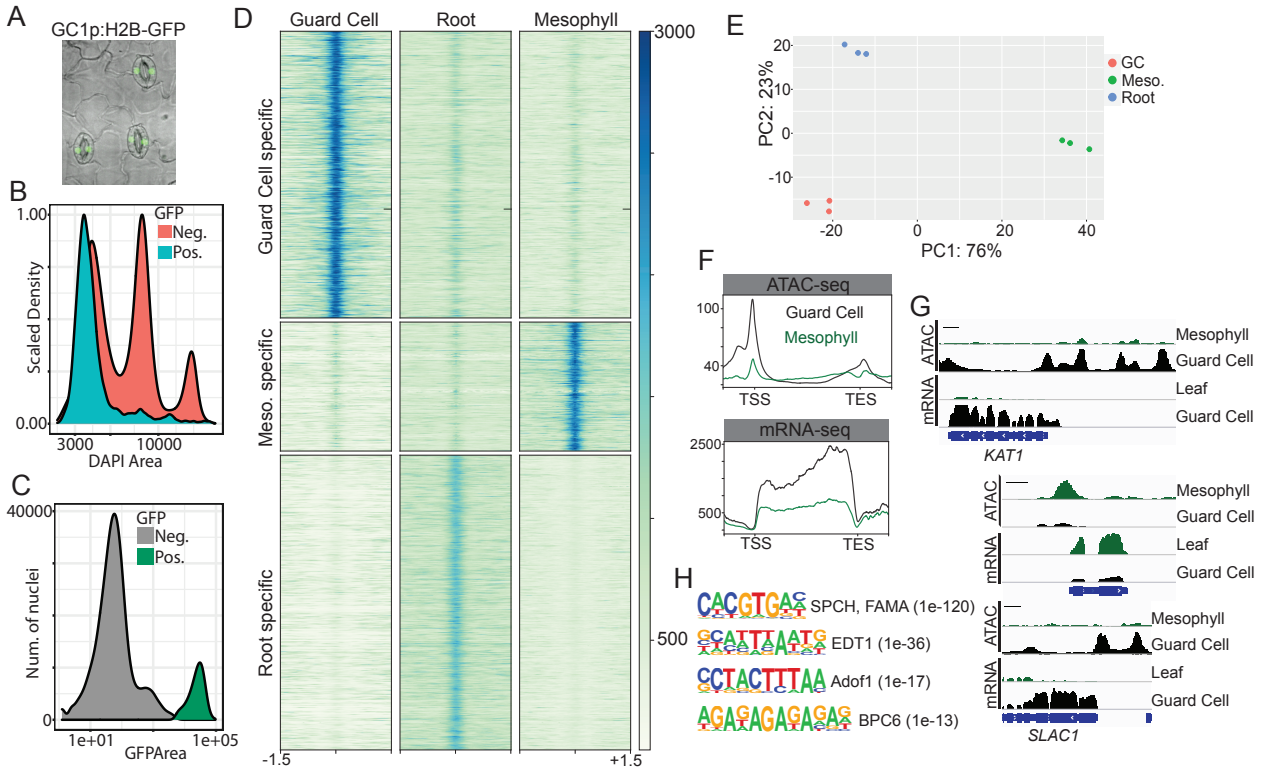

Fig 2. Cell-type specific epigenomics identifies guard cell specific regulatory elements. **A)** Volcano plot of differential ATACseq analysis showing regions that significantly change in chromatin accessibility in seedlings after 4hrs of ABA treatment. ABA increased accessibility at 638 regions and decreased accessibility at 372 regions (FDR < 0.01 and FC > 1.5). **B)** Heatmap of root nuclei ATAC-seq signal at regions showing ABA-regulated chromatin accessibility over the indicated ABA treatment time course. **C)** Number of ABA-regulated ATAC-seq peaks over time in roots. Bars summarizing ABA-induced peaks are colored in blue while bars representing ABA-repressed peaks are colored in pink. **D)** Genomic distribution among annotated features of all ATAC-seq peaks (orange) and in ABA-regulated ATAC-seq peaks (grey). **E)** Genome browser snapshots at three representative genes showing the change in ATAC-seq signal in upstream regions following ABA treatment. **F)** The transcription factor binding motifs with the highest enrichment in ABA-induced and ABA-repressed chromatin regions in roots.

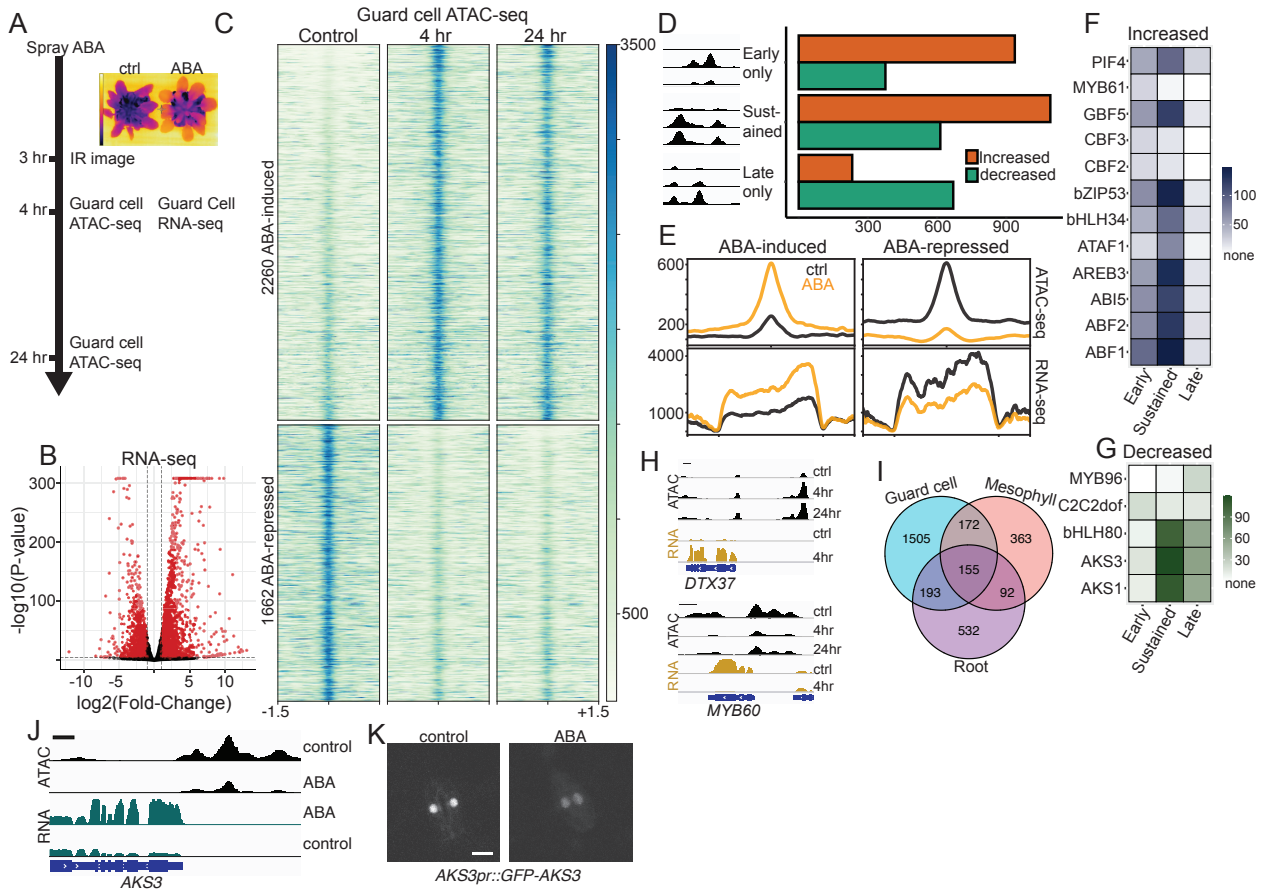

Figure 3. ABA triggers extensive and persistent chromatin remodeling in guard cells. **A)** Schematic showing the experimental outline. Plants were sprayed with ABA and infrared images were taken using a thermal camera to assess stomatal closure. Guard cell nuclei were purified at 4hrs and 24 hrs after treatment and used for ATAC-seq. **B)** Volcano plot of guard cell enriched RNA-seq data showing ABA upregulates 2134 transcripts and downregulates 1452 transcripts. **C)** Heatmap of ATAC-seq signal in guard cell nuclei centered over 2260 regions with ABA-induced chromatin accessibility and 1662 regions with ABA-repressed chromatin accessibility (FDR < 0.001, FC > 2.0). **D)** Comparison of ABA-regulated peaks from 4hr and 24hr after treatment separated regions into three categories – early only, sustained (both early and late), and late only. The bar graph shows the number of ABA-increased and -decreased regions in each category. **E)** ATAC-seq and RNA-seq metaplots showing average chromatin accessibility and transcript levels near ABA-induced and ABA-repressed ATAC-seq peaks. **F,G)** Heatmap showing the results of homer motif analysis of ABA-increased **(F)** and ABA-decreased **(G)** ATAC-seq peaks. **H)** Genome browser images showing guard cell ATAC-seq and RNA-seq coverage at a representative ABA-induced gene (*DTX37)* and an ABA-repressed gene (*MYB60*). **I)** Overlap of ABA-induced accessible regions in guard cell nuclei, mesophyll nuclei, and root nuclei. **J)** Genome browser images showing guard cell ATAC-seq and RNA-seq coverage at *AKS3*. **K)** Fluorescence micrograph showing expression of *AKS3pr::GFP-AKS3* in guard cells after treatment with control or ABA (4 hr).

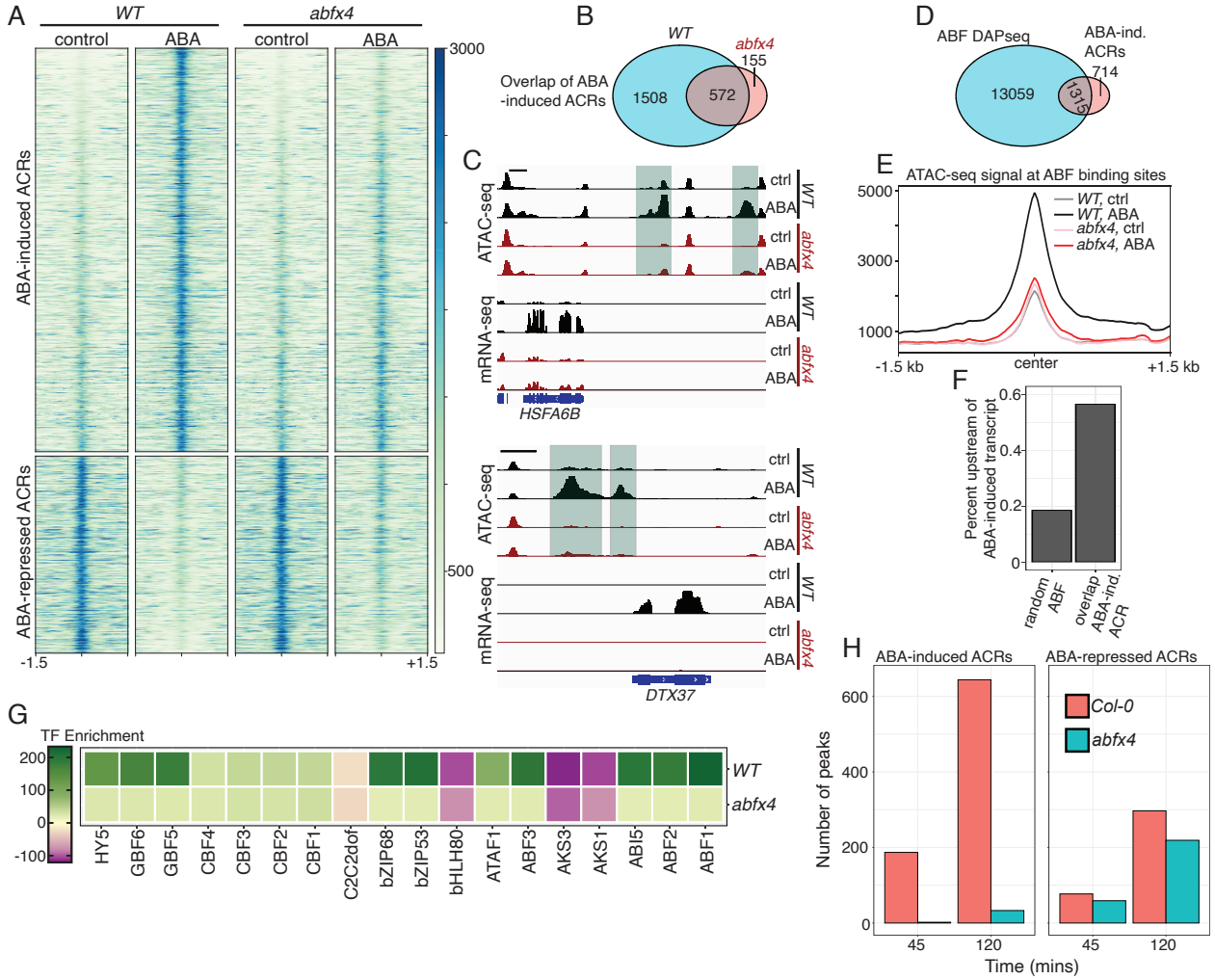

Fig 4. ABF transcription factors are required for ABA-induced chromatin opening in guard cells. A) Heatmap of ATAC-seq signal in either *WT* or *abfx4* mutant guard cells at 2029 regions with ABA-induced accessibility and 991 regions with ABA-repressed accessibility (FDR < 0.01 and FC > 2.0). **B)** Overlap of ABA-induced ATAC-seq peaks in *WT* guard cells with those in *abfx4* mutant guard cells. **C)** Genome browser snapshots showing ATAC-seq and RNA-seq signal near two ABA-induced genes *DTX37* and *HSGA6B*. **D)** Overlap between ABF DAP-seq peaks (Sun et al 2022) and ABA-induced accessible chromatin regions (ACRs). **E)** Peak metaplot showing ATAC-seq signal in the indicated samples at ABA-induced ATAC-seq peaks containing ABF DAP-seq binding sites. **F)** 1315 ABF-DAP-seq peaks overlapping ABA-induced ATAC-seq peaks or 1315 random ABF DAP-seq binding sites were assigned to nearest upstream genes. The plot shows the percentage of these genes that are transcriptionally induced by ABA treatment. **G)** Enrichment (-log P_value) of the indicated transcription factor binding motifs in ABA regulated ATAC-seq peaks in either *WT* or *abfx4* mutant guard cell nuclei. Negative enrichment scores indicate motifs overrepresented in condition-repressed regions. **H)** Bar plots representing the number of ABA-activated or ABA-repressed ACRs over time in *Col-0* or *abfx4* mutant roots.

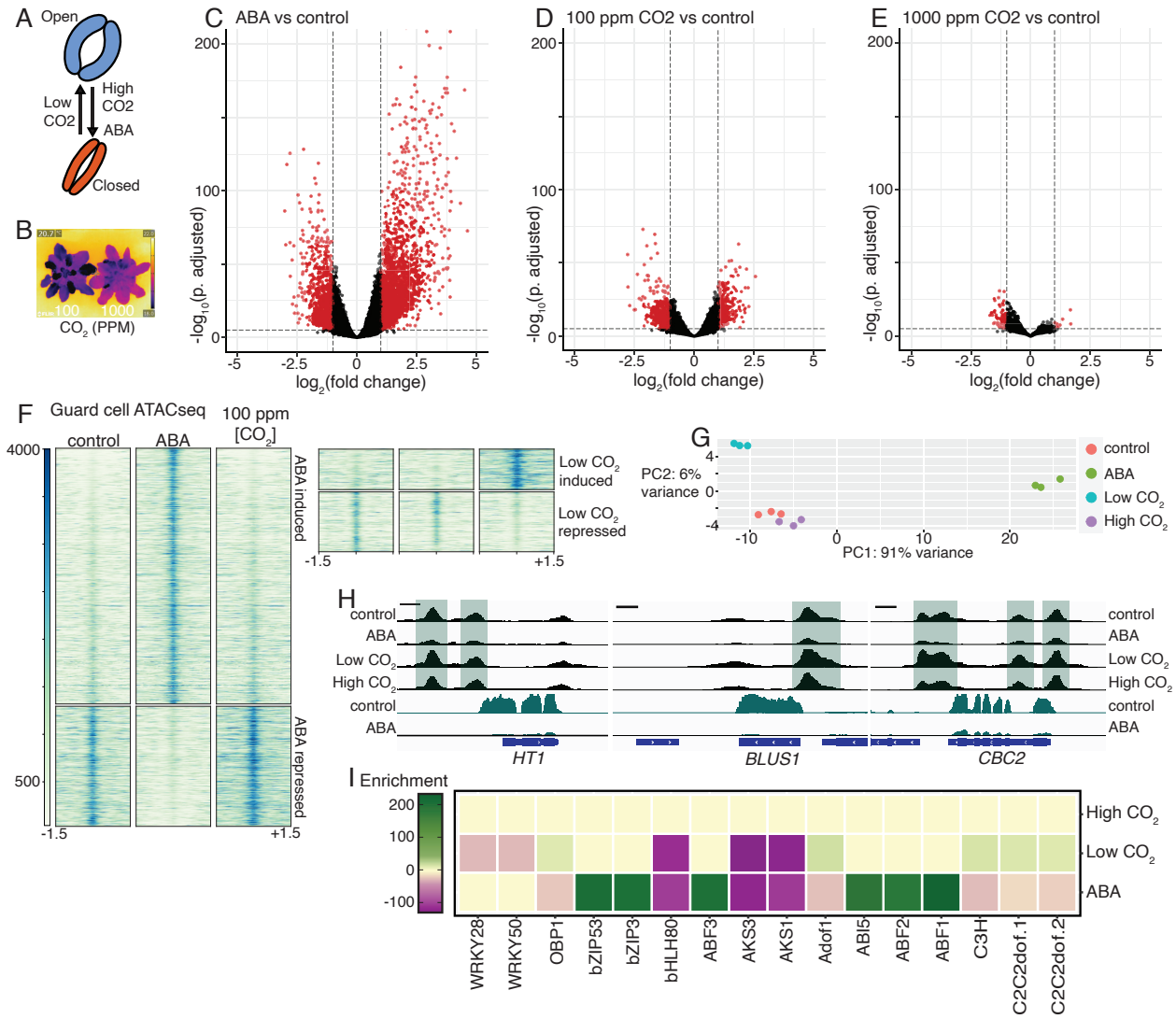

Fig 5. ABA and changes in CO_2 concentration induce distinct chromatin remodeling programs in guard cells. A) Diagram showing the effects of different stimuli on the stomatal aperture. **B)** Representative IR image showing differences in leaf temperature due to CO_2 induced stomatal movement. **C-E)** Volcano plots of ATAC-seq data showing **C)** ABA-regulated chromatin accessibility, **D)** low CO_2 regulated chromatin accessibility, and **E)** high CO2 regulated chromatin accessibility. The number of differentially accessible peaks (colored in red, FDR < 0.01 and FC > 2.0) in each condition is indicated on each plot. **F)** Heatmaps of guard cell ATAC-seq signal centered over ABA-regulated ACRs (2029 induced and 991 repressed) and low CO_2-regulated ACRs (329 induced and 487 repressed). Libraries are derived from plants exposed to the indicated treatments. **G)** Principle component analysis (PCA) shows that ABA, low CO_2, and high CO_2 introduce separate variation to genome-wide chromatin accessibility. **H)** Genome browser snapshots showing ABA-repression of chromatin accessibility upstream of HT1, BLUS1, and CBC1 – three positive regulators of low CO_2 induced stomatal opening. **I)** Enrichment (-log P_value) of the indicated transcription factor binding motifs in ABA, Low CO2, or High CO_2 regulated regions. Negative enrichment scores indicate motifs overrepresented in condition-repressed regions.
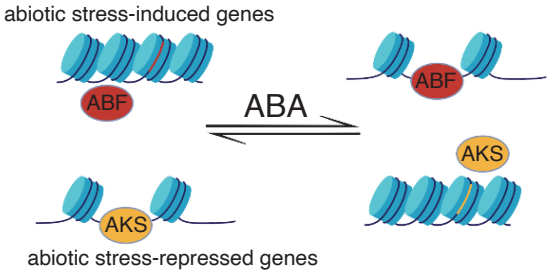
Fig. 6 Model - ABA regulates opposing chromatin states in guard cells. In unstressed guard cells, AKS proteins maintain open chromatin at ABA-repressed genes while ABA-induced genes are kept silent by closed chromatin at their upstream regulatory regions. During abiotic stress, SnRK2s activate ABFs and inhibit AKSs. This leads to the establishment of open chromatin at stress-activated genes and the silencing of ABA-repressed genes by the closing of chromatin.